ANL/NE-13/11

Argonne NATIONAL LABORATORY

Development of SFR Primary System Simulation Capability for Advanced System Codes

Nuclear Engineering Division

ANL/NE-13/11

Development of SFR Primary System Simulation Capability for Advanced System Codes

by
R. Hu, J. W. Thomas, E. Munkhzul, and T. H. Fanning
Nuclear Engineering Division, Argonne National Laboratory

H. Zhang and R. Martineau
Idaho National Laboratory

September 30, 2013

EXECUTIVE SUMMARY

Under the Reactor Product Line (RPL) of DOE/NE's Nuclear Energy Advanced Modeling and Simulation (NEAMS) program, an SFR System Analysis Module is being developed at Argonne National Laboratory for whole-plant safety analysis. This tool will simulate tightly coupled physical phenomena – including nuclear fission, heat transfer, fluid dynamics, and thermal-mechanical response – in SFR structures, systems, and components. It is based on the MOOSE (Multi-physics Object-Oriented Simulation Environment) framework, which relies upon open-source libraries such as libMesh and PETSc for mesh generation, finite element analysis, and numerical solutions. This development is a coordinated effort along with the development of RELAP-7, which is an advanced safety analysis tool for light-water reactors developed at Idaho National Laboratory. The SFR Module is aimed to model and simulate the SFR systems with much higher fidelity and with well-defined and validated prediction capabilities. It will provide fast-running, modest-fidelity, whole-plant transient analyses capability, which is essential for fast turnaround design scoping and engineering analyses.

The SFR System Module is being built based on RELAP-7 and the MOOSE framework. It leverages the common features between LWRs and SFRs (e.g., single-phase flow in a pipe and steam-system modeling for the balance of plant). The existing RELAP-7 physics models and component library are directly available for use in the SFR System Module. On the other hand, the SFR Module effort assists with RELAP-7 development by providing code verification and contributing general physics models and components applicable to all reactor types.

Although the MOOSE and RELAP-7 based SFR system analysis module is a relative new effort (less than two years), significant accomplishments have been achieved. A 1-D FEM flow model using a pressure-based formulation with numerical stabilization schemes has been developed for use in incompressible sodium flows. A set of SFR-specific physics models and component has also been developed. The SFR primary system simulation capabilities of the SFR Module have been demonstrated by simulating the early stage of the Protected Loss-Of-Flow (PLOF) accident in the Advanced Burner Test Reactor (ABTR). Both the steady-state and PLOF transient simulation results are compared with the SAS4A/SASSYS-1 simulation results. It is confirmed that major physics phenomena in the primary coolant loop during the transient can be captured by the SFR Module.

The SFR Module also emphasizes providing multi-scale multi-physics modeling capabilities by integrating with other higher-fidelity advanced simulation tools. This investigation is important to the integration between the MOOSE-based system code and the high-fidelity and medium-fidelity advanced simulation capabilities developed under the NEAMS RPL. The multi-scale coupling capability has been demonstrated in the coupled SFR Module and STAR-CCM+ code simulation of the ABTR PLOF transient. The importance of the multi-resolution capability was demonstrated by the multi-dimensional flow and the formation of thermal stratification layers in the outlet plenum and cold pool of the ABTR during the postulated transient. Although the general trends of transient evolutions are similar, very different flow rates and temperatures are predicted among the stand-alone SFR Module, stand-alone SAS4A/SASSYS-1, and the coupled SFR Module and STAR-CCM+ simulations because of the differences in modeling the mixing and thermal stratification in the large

sodium pools. In the transient simulation of ABTR PLOF, the effects of "component-to-component" heat transfer, cold pool stratification, the modeling of upper internal structure (UIS), and the time-step size, have also been investigated. It is found that the PLOF transient response of the pool-type ABTR is sensitive to all these modeling choices. Therefore, detailed CFD models of the cold pool, the hot pool, the redan wall, and the UIS are necessary for accurate predictions of the transient evolution in the coupled system and CFD code simulation of the ABTR PLOF.

The SFR Module developmental efforts and the progress so far are very encouraging. The next stage of the development will focus on the continuous development of physics modeling and component designs for SFR analysis, the possible integration between the pressure-based formulation and the density-based FEM flow formulation in RELAP-7, the advanced preconditioning techniques and alternative numerical integration schemes other than Jacobian-Free Newton–Krylov (JFNK) methods for improved code execution speed. Additionally, the integration with other high-fidelity advanced simulation tools developed under the NEAMS Program, such as Nek-5000, will be investigated.

TABLE OF CONTENTS

LIST OF FIGURES

LIST OF TABLES

1 Introduction

An advanced system analysis tool is being developed at Argonne National Laboratory for sodium fast reactor (SFR) simulations under the Reactor Product Line (RPL) of DOE/NE's Nuclear Energy Advanced Modeling and Simulation (NEAMS) program. This tool solves the tightly-coupled physical phenomena including fission reaction, heat transfer, fluid dynamics, and thermal-mechanical response in the SFR structures, systems, and components. It is based on the MOOSE (Multi-physics Object-Oriented Simulation Environment) framework [1], which is subsequently based on libMesh [2] and PETSc [3] for meshing capabilities, numerical methods of finite element analysis, and non-linear solvers. This development is a coordinated effort along with the development of RELAP-7 [4], which is an advanced safety analysis tool for light-water reactors developed at Idaho National Laboratory.

With advances in numerical techniques and software engineering, such as the availability of PETSc and MOOSE, modernization of existing systems codes or the development of new system codes becomes more compelling. RELAP-7 uses the MOOSE object oriented framework to interface with libMesh and PETSc to provide the underlying geometry and numerical capabilities, while RELAP-7 itself defines objects on this interface that represent typical components and systems in a light water reactor (LWR). In collaboration with the developments for RELAP-7, additional developments are needed for components and systems that represent typical features of advanced reactor concepts such as SFRs, LFRs, and FHRs. These advanced concepts are distinguished from light-water reactors in their use of single-phase, low-pressure, very low Prandtl number coolants. This simple yet fundamental change has significant impacts on core and plant design, the types of materials used, component design and operation, fuel behavior, and the significance of the fundamental physics in play during transient plant simulations. These parallel development efforts are referred to as the SFR Module to highlight its current focus and to distinguish the modeling needs of advanced reactor concepts from light-water reactors.

This report discusses the initial developments of the one-dimensional systems-level simulation capabilities for the SFR Module. The RELAP-7 development is described first in Section 2 since the SFR Module is built around RELAP-7 and the MOOSE framework. The code development approach and current capabilities are discussed in Section 3. The developed multi-scale code coupling capability between the SFR Module and the CFD code STAR-CCM+ [5] is also included, since the multi-scale, multi-resolution approach is one of the key objectives being pursued within the NEAMS RPL. Section 4 describes the demonstration simulation of the SFR Module for the Advance Burner Test Reactor (ABTR) [6]. Both the steady state and the Protected Loss Of Flow (PLOF) transient simulations are discussed. The SAS4A/SASSYS-1 [7] simulation results are also included for comparison. Furthermore, the coupled SFR Module and STAR-CCM+ code simulation of ABTR PLOF transient is discussed in Section 5. The effects of the time-step size and the modeling of the upper core structures in the coupled code simulation are also discussed. Finally, Section 6 provides a summary of the FY13 effort and future work.

2 Overview of Relap-7 Code Development

2.1 Objectives

The RELAP-7 (Reactor Excursion and Leak Analysis Program) code is the next generation of nuclear reactor system safety analysis code being developed at the Idaho National Laboratory [4]. RELAP-7 will become the main reactor systems simulation toolkit for the Risk Informed Safety Margin Characterization Pathway of the DOE's Light Water Reactor Sustainability Program and the next generation tool in the RELAP reactor safety/systems analysis application series (i.e., the replacement for RELAP5). The RELAP-7 code development is taking advantage of the progresses made in the past several decades to achieve simultaneous advancement in physical models, numerical methods, and software design. RELAP 7 utilizes the Idaho National Laboratory's MOOSE (Multi-Physics Object-Oriented Simulation Environment) framework [1] for solving computational engineering problems in a well-planned, managed, and coordinated way. This allows restriction of the focus of RELAP-7 to systems analysis-type physical modeling and gives priority to retention and extension of RELAP5's [8] capabilities.

2.2 Overview of Current Capabilities

Software Framework: RELAP-7 is the MOOSE-based application for reactor systems analysis. MOOSE significantly reduces the expense and time required to develop RELAP-7. Numerical methods, mesh management, and parallel computational controls are all provided within MOOSE. Therefore, with MOOSE providing the heavy computational lifting, RELAP-7 code developers only need to focus on physics, numerical algorithm, and the user interface and capability. This has greatly enhanced the productivity and promoted rapid code development. RELAP-7 code is being developed following the same modern software design paradigms used for MOOSE development. There are currently over 20 different MOOSE-based applications ranging from 3-D transient neutron transport, detailed 3-D transient fuel performance analysis, to long-term material aging. Multi-physics and multiple dimensional analyses capabilities can be obtained by coupling RELAP-7 and other MOOSE-based applications and/or by leveraging capabilities developed by other DOE programs. This allows restricting the focus of RELAP-7 to systems analysis-type simulations and gives priority to retain and significantly extend RELAP5's capabilities.

Governing Theory: The fluids flow, heat transfer, and reactor kinetics models are the basis of RELAP-7 governing theory. While RELAP-7 is envisioned to incorporate both single and two-phase coolant flow simulation capabilities encompassing all-speed and all-fluids, the main focus in the immediate future of RELAP-7 development is LWRs. Since the interest of this milestone is for SFR application, only the single phase flow models are described here. The single phase flow models in RELAP-7 employ the 1-Dimensional conservation equations of mass, momentum and energy. Hence three partial differential equations (PDE) are developed and solved. The conservative form of the PDEs are developed and solved in order to better capture the pressure wave effects in a reactor system. Additionally the compressible flow models are used in RELAP-7. RELAP-7 also simulates the heat transfer process as well reactor kinetics as the heat source. The heat-conduction equation for cylindrical or slab geometries is solved to provide thermal history within metal structures such as fuel and clad. The volumetric power source in the heat conduction equation for the fuel comes from the

point kinetics model with thermal hydraulic reactivity feedback considered. The reactor structure is coupled with the thermal fluid through energy exchange between them (conjugate heat transfer) by the surface convective heat transfer. The fluid, heat conduction, conjugate heat transfer and point kinetics equations are solved in a fully coupled fashion in RELAP-7 in contrast to the operator-splitting or loose coupling approach used in the existing system safety analysis codes.

Computational Approach: With an all-speed and all-fluids goal in mind, RELAP-7 is also being designed to handle any systems level transient imaginable. This can cover the typical design basis accident scenarios (on the order of one second time scales) commonly associated with RELAP5 simulations to reactor core fuel burnup simulations (on the order of one year time scales). Unfortunately, the JFNK algorithm can be inefficient in both of these time scale extremes. For short duration transients, typically found in RELAP5 simulations, the JFNK approach requires a significant amount of computational effort be expended for each time step. If the simulation requires short time steps to resolve the physics coupling, JFNK may not be necessary to resolve the nonlinear coupling. The Pressure-Corrected Implicit Continuous-fluid Eulerian (PCICE) algorithm [9][10][11] is an operator-split semi-implicit time integration method that has some similarities with RELAP5's time integration method but does not suffer from phase and amplitude errors, given a stable time step. Conversely for very long duration transients, JFNK may not converge for very large time steps as the method relies on resolving the nonlinear coupling terms, and thus, may require an initial estimate of the solution close to the advanced solution time which maybe unavailable. Recently, a point implicit time integration method has been developed for slow transient flow problems. If successfully integrated into the MOOSE framework, this slow transient capability would be available to RELAP-7. Thus, a three-level time integration approach is being pursued to yield an all-time scale capability for RELAP-7. The three integration approaches are described as follows:

1. The PCICE computational fluid dynamics (CFD) scheme, developed for all-speed compressible and nearly incompressible flows, improves upon previous pressure-based semi-implicit methods in terms of accuracy and numerical efficiency with a wider range of applicability. The PCICE algorithm combined with the Finite Element Method (FEM) spatial discretization scheme yields a semi-implicit pressure-based scheme called the PCICE-FEM scheme. In the PCICE algorithm, the total energy equation is sufficiently coupled to the pressure Poisson equation to avoid iteration between the pressure Poisson equation and the pressure-correction equations. Both the mass conservation and total energy equations are explicitly convected with the time-advanced explicit momentum. The pressure Poisson equation then has the time-advanced internal energy information it requires to yield an accurate implicit pressure. At the end of a time step, the conserved values of mass, momentum, and total energy are all pressure-corrected. As a result, the iterative process usually associated with pressure-based schemes is not required. This aspect is highly advantageous when computing transient flows that are highly compressible and/or contain significant energy deposition, chemical reactions, or phase change.

2. The JFNK method easily allows implicit nonlinear coupling of dependent physics under one general computational framework. Beside rapid (second-order) convergence of the iterative procedure, the JFNK method is flexible in its ability to handle multiphysics problems when time scales of different physics are significantly varied during transients. The key

feature of the JFNK method is combining Newton's method to solve implicit nonlinear systems with Krylov subspace iterative methods. The Krylov methods do not require an explicit form of the Jacobian, which eliminates the computationally expensive step of forming Jacobian matrices (which also may be quite difficult to determine analytically) required by Newton's method. The matrix-vector product can be approximated by the numerical differentiation of nonlinear residual functions. Therefore, JFNK readily integrates different physics into one solver framework.

3. Semi-implicit and nonlinear implicit methods can step over certain fine time scales (i.e., ones associated with the acoustic waves), but they still have to follow material Courant time stepping criteria for stability or convergence purposes. The new point implicit method is devised to overcome these difficulties [12]. The method treats the solution variables of interest (that can be located at cell centers, cell edges, or cell nodes) implicitly, and the rest of the information related to same or other variables are handled explicitly. The point-wise implicit terms are expanded in Taylor series with respect to the explicit version of the same terms, at the same locations, resulting in a time marching method that is similar to the explicit methods and, unlike the fully implicit methods, does not require implicit iterations. This new method shares the characteristics of the robust implementation of explicit methods and the stability properties of the unconditionally stable implicit methods. This method is specifically designed for slow transient flow problems wherein, for efficiency, one would like to perform time integrations with very large time steps. Researchers at the INL have found that the method can be time inaccurate for fast transient problems, particularly with larger time steps. Therefore, an appropriate solution strategy for a problem that evolves from a fast to a slow transient would be to integrate the fast transient with a semi-implicit or implicit nonlinear technique and then switch to this point implicit method as soon as the time variation slows sufficiently. A major benefit of this strategy for nuclear reactor applications will reveal itself when fast response coolant flow is coupled to slow response heat conduction structures for a long duration, slow transient. In this scenario, as a result of the stable nature of numerical solution techniques for heat conduction one can time integrate the heat part with very large (implicit) time steps.

2.3 Updates in Single-Phase Flow Modeling

A real reactor system is very complex and may contain hundreds of different physical components. Therefore, it is impractical to preserve real geometry for the whole system. Instead, simplified thermal hydraulic models are used to represent (via "nodalization") the major physical components and describe major physical processes (such as fluid flow and heat transfer). There are three main types of components developed in RELAP-7: (1) one-dimensional (1-D) components, (2) zero-dimensional (0-D) components for setting a boundary, and (3) 0-D components for connecting 1-D components. Table 1 shows the major components developed for single phase flow analyses.

Table 1. Major RELAP-7 components for single phase analysis.

Component name	Descriptions	Dimension
Pipe	1-D fluid flow within 1-D solid structure with wall friction and heat transfer	1-D
CoreChannel	Simulating reactor flow channel and fuel rod, including 1-D flow and 1-D or two-dimensional (2-D) fuel rod heat conduction	1-D
HeatExchanger	Co-current or counter-current heat exchanger model, including fluid flow in two sides and heat conduction through the solid wall	1-D
PipeWithHeatStructure	Simulating the fluid flow associated with a solid heat structure, including fluid flow, solid heat conduction with different boundary conditions	1-D
TimeDependentVolume	Provides pressure, temperature, and void fraction boundary conditions for 1-D components	0-D
TimeDependentJunction	Provides velocity, temperature, and void fraction boundary conditions for 1-D components	0-D
TDM	Time dependent mass flow, which provides mass flow boundary for 1-D components	0-D
Branch	Multiple inlets and outlets 0-D junction, which provides form loss coefficients (K)	0-D
Pump	A junction model with momentum source connecting two 1-D components	0-D
PointKinetics	Point kinetics neutronics model	0-D
DownComer	Large volume to mix different streams of water and steam and to track the water level	0-D
Valve	Simulate control mechanisms of real valves in a hydrodynamic system	0-D
Reactor	A virtual component that allows users to input the reactor power	0-D

Pipe is the most basic component in RELAP-7. Thermal fluid dynamic equations are solved for this component. Wall friction factor and convective heat transfer coefficient are calculated through closure laws or provided by user inputs. Gravity effect is taken into account by the pipe orientation and flow direction.

CoreChannel is a composite component designed to simulate both fluid flow and heat conduction inside a fuel rod. The fuel rod is divided into the same number of segments as the number of fluid flow pipe elements. Each rod segment is further simulated as 1-D thermal conduction model perpendicular to the fluid flow model. Both plate type of fuel rod and cylindrical fuel rod can be simulated. The flow model and conduction model are strongly coupled instead of loosely coupled as in RELAP5.

A simple *HeatExchanger* model is a combination of two fluids and one heat structure. This will be expanded into a more complicated steam generator model in the future.

PipeWithHeatStructure is another composite component, which simulates 1-D fluid flow and 2-D heat structure. Different boundary conditions on the outside solid boundary can be applied. Either plate or cylinder type of heat structure can be simulated. Volumetric heating within fluid or solid can be added.

Time dependent volume is a component that provides a time dependent pressure and temperature boundary conditions to its neighbor. It is a pure boundary condition type of component without any number of degrees, i.e., it doesn't add any entries to the global unknown vector. When acquired by its connected 1-D component, it provides a pressure and a temperature boundary condition. *Time dependent junction* and *Tdm* (time dependent mass flow rate) have similar functions with different boundary condition types.

A *Branch* is basically a junction with multiple inlets and outlets. Branch has single/multiple inlets and single/multiple outlets, of which cross-section areas can be different.

A simple *Pump* can be treated as a single junction with momentum source. It connects two pipes. For steady state along positive flow direction, the pump model provides a nominal pump head. For reverse flow, the pump has large flow resistance; a form loss K inputted by users should be used.

A *PointKinetics* model is a lumped parameter neutronics model to calculate the reactor thermal power. Fully coupled thermal hydraulic feedback reactivity model has been implemented for the PointKinetics model.

A *Downcomer* model provides the mixing of different streams of coolant such as feed water flow, etc.

A *Valve* model is derived from a branch model with controllable flow area and resistance to realize its functions. The current valve component developed in RELAP-7 is a simplified model to simulate the fundamental functions (i.e. open and close) of generic valves. The valve component is a junction type of components and it connects one pipe on each side. The valve is initiated with a user given status (i.e., fully open or fully closed). It then starts to react (i.e., close or open) and is triggered either by a preset user given trigger time or by a trigger event. In its opening status, either fully open or partially open, it serves as a regular flow junction with form losses. In its fully closed status, the connected two pipes are physically isolated. The current valve model also includes the gradually open/close capability similar to a motor driven valve to simulate the physical behavior of a valve open/close procedure.

The *Reactor* component is a virtual component added in RELAP-7 to allow users to specify the reactor power (i.e., steady-state power or decay heat curve) or heat source. Either the *Reactor* component or the *PointKinetics* component (but not both) can used to provide the reactor power used in the RELAP-7 calculations.

3 Code Developments for SFR System Modeling

3.1 *Development Approach*

The SFR Module is aimed to model and simulate the SFR systems with much higher fidelity and with well-defined and validated prediction capabilities. It will provide fast-running, modest-fidelity, whole-plant transient analyses capability, which is essential for fast turnaround design scoping and engineering analyses and could lead to improvements in the design of new reactors, the reduction of uncertainties in safety analysis, and reductions in capital costs. To fulfill its objectives, the SFR Module

- Utilizes the MOOSE framework to leverage the available advanced software environments and numerical methods.
- Incorporates advances in the physical and empirical models for SFR system analysis developed over the past several decades.
- Provides multi-scale multi-physics modeling capabilities by integrating with other higher-fidelity advanced simulation tools.

The SFR Module is being built around RELAP-7 and the MOOSE framework (see Figure 1). It leverages the common features between LWRs and SFRs (e.g. single-phase flow in a pipe and steam-system modeling for the balance of plant). The existing RELAP-7 physics models and component library are directly available for use in the SFR Module as dependent libraries. Additionally, this program

- Collaborates on RELAP-7 development by providing code verification and contributing general physics models and components applicable to all reactor types.
- Developed a 1-D FEM flow model using a primitive variable based formulation with numerical stabilization schemes for use in incompressible sodium flows.
- Developed a multi-scale, single-phase flow coupling capability between the SFR Module and the CFD code STAR-CCM+ to simulate the multidimensional phenomena.
- Develops SFR-specific physics models and components based on both the conservative-variable based (RELAP-7) flow model and the primitive variable based formulation.
- Develops advanced physics models and components compatible and available for use in RELAP-7.
- Develops demonstration problems for the newly added stand-alone system simulation capabilities and coupled multi-scale or multi-physics simulation capabilities.

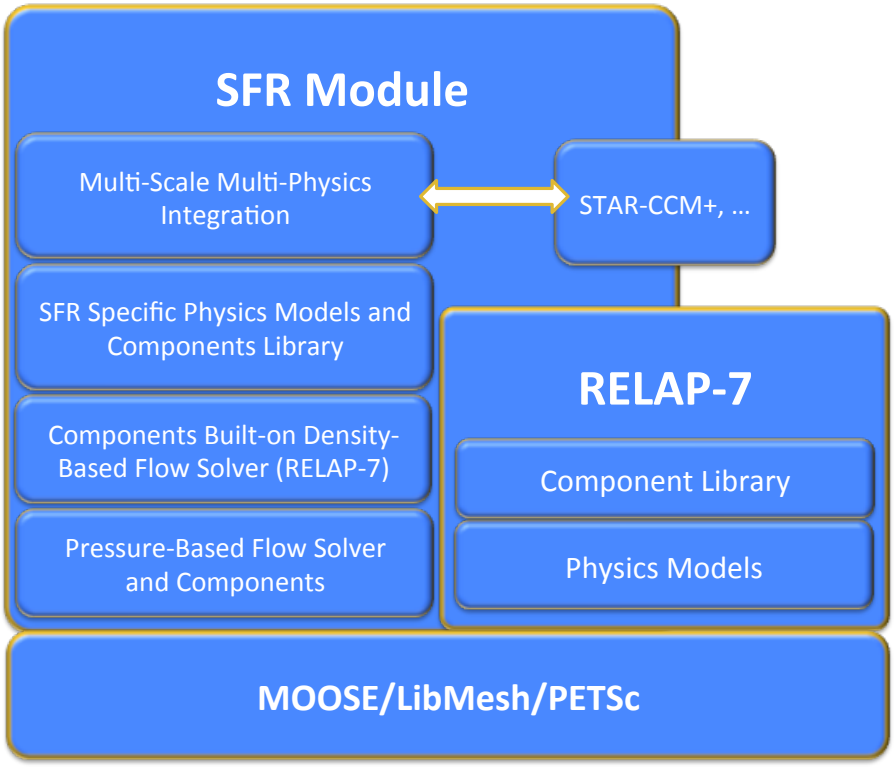

Figure 1: The Structure of the SFR System Analysis Module

3.2 *Overview of Current Capabilities*

To develop a system analysis code, numerical methods, mesh management, equation of states, fluid properties, solid material properties, neutronics properties, pressure loss and heat transfer closure laws, and good user input/output interfaces are all indispensible. The SFR Module leverages the MOOSE and RELAP-7 effort, thus the existing features of MOOSE and Relap-7 are integrated into the capabilities of the SFR Module, including the JFNK solver schemes, the mesh management, some reactor component models, and the I/O interfaces, etc. The current capabilities of the RELAP-7 code, described in Section 2, are directly available for use in the SFR Module. Additionally, new physics and component models are developed to model some unique features of SFR system.

3.2.1 Primitive Variable based Finite Element Formulation

Parallel to RELAP-7 development, numerically stable schemes for continuous finite element analysis of single-phase flow have been developed for non-LWR advanced reactor applications based on the MOOSE framework. It uses primitive variable (or pressure) based formulation, while the RELAP-7 code uses the conservative variable (or density) based formulations in one-dimension Finite Element method. Although the conservative variable based formulation has many advantages in the applications of compressible flow such as the capability to capture the shock waves, the primitive variable based FEM formulation would be more suitable for incompressible or nearly incompressible flows, such as the fluid flow in the SFRs, LFRs, or FHRs. To prevent the potential numerical instability issues, the stabilization techniques of incompressible flows were extensively reviewed, and the

Streamline-Upwind Petrov-Galerkin (SUPG) and the Pressure-Stabilizing Petrov-Galerkin (PSPG) formulations [13] have been chosen and implemented as the stabilization schemes.

The developed primitive variable based finite element fluid model has been examined and verified by several channel flow test problems. This model can be used as a substitute to the conservative variable formulation in RELAP-7 for incompressible flows. For fast development of SFR primary system simulation capability, significant effort was focused on the development of component using the conservative variable based formulations in FY13 since it is consistent with the current RELAP-7 code framework. However, the possible integration between the primitive variable and the conservative variable based formulations will be addressed in FY14.

3.2.2 Sodium Property and Equation of State

The sodium property model in SAS4A/SASSYS-1 [7] is applied in the SFR Module. In this model, most sodium properties are dependent on temperature only, including heat capacity, thermal conductivity, viscosity, compressibility, and thermal expansion coefficient, etc.

A new sodium Equation Of State (EOS) model is developed to complete the flow governing equations. This development is based on the conservative variable formulation in RELAP-7. Therefore, the pressure and temperature dependencies on the state variables ($\rho, \rho u,$ and ρE) and their partial derivatives are developed in the EOS model. A reference state is required for the model, which can be provided from the user input. This EOS model is developed based on the Non-Isothermal EOS model in RELAP-7, in which the fluid is compressible and the material properties are constant.

3.2.3 Constitutive Laws

Empirical correlations for friction factor and heat transfer coefficient have been implemented in the SFR Module. The friction and heat transfer coefficients are then dependent on flow conditions during the transient. The McAdams and Blasius correlations [14] are used for the wall friction factor, and the Seban and Shimazaki correlation [14] is used for liquid metal heat transfer coefficient. These correlations were the same as those implemented in SAS4A/SASSYS-1.

$$\begin{aligned} f &= 0.316\, Re^{-0.25}\,, \; 2100 < Re < 3\times10^4 \\ &= 0.184\, Re^{-0.2}\;\;, \; 3\times10^4 < Re < 2\times10^6 \end{aligned} \tag{1}$$

$$Nu = 5.0 + 0.025\, Pe^{0.8} \tag{2}$$

3.2.4 Component Modeling and Physics Integration

Similar to RELAP-7, the physics modeling and mesh generation of individual reactor components were encapsulated as Component classes. A simple set of components was developed using the primitive variable based FEM formulation as the first attempt to develop system analysis capability in the MOOSE framework. However, the effort was shifted to develop components using the conservative variable based formulation for the fluid flow, for

the purpose of 1) obtaining the SFR primary system modeling capability in a shorter time, and 2) enhancing the collaboration with the RELAP-7 effort.

The RELAP-7 code has mainly three types of components: (1) 1-D components such as pipe, core channel, and heat exchanger; (2) 0-D components for setting boundary conditions such as time dependent volume, time dependent junction, and time dependent mass flow rate; and (3) 0-D components for connecting 1-D components such as junction/branch and pumps. Based on the fluid flow (conservative variable formulation) model in RELAP-7, additional components and physics models have been developed for the SFR system modeling due to the fundamental design differences between the SFRs and LWRs, as listed in Table 2.

Table 2. Major SFR Module Components, based on the conservative variable formulation

Component name	Descriptions	Dimension
CoreChannelwDuct	Simulating reactor core channel, including 1-D flow channel, the inner heat structure of the fuel rod, and the outer heat structure of the duct wall.	1-D
BypassChannel	Developed to model the bypass flow in the gaps between fuel assemblies.	1-D
ReactorCore	Model a pseudo three-dimensional reactor core; It consists of member core channels (with duct walls) and bypass channels.	0-D
PresetPump	Derived from the Pump component, but the pump head is dependent on a pre-defined function.	0-D
CoverGas	A 0-D gas volume that is connected to one or multiple liquid volumes.	0-D
LiquidVolumeWithCoverGas	The 0-D liquid volume with cover gas, thus the liquid volume can change during the transient.	0-D
HeatStructureWithLiquidVolume	The heat structure connected two liquid volumes. Developed to model the heat transfer between two 0-D components.	1-D, 2-D or 3-D
CoupledTDV	A TimeDependentVolume boundary in which the boundary conditions are provided by other codes in coupled code simulation.	0-D
VolumeBranch*	Considering the volume effects of a flow joint so that it can account for the mass and energy in-balance between the inlets and outlets due to inertia	0-D

PipeWithHeatStructure*	Simulating the fluid flow in a pipe, the heat conduction in the pipe wall, and the heat transfer at inner and outer pipe walls.	1-D

*: Incorporated into the RELAP-7 components.

The developed components provides two major modeling features:

1. A three-dimensional capability to model the heat-transfer in the reactor core. The heat generated in the fuel rod of one fuel assembly can be transferred to the coolant in the core channel, the duct wall, the inter-assembly gap, and then the adjacent fuel assemblies. This is particularly important for SFR since the thermal conductivity of the sodium is very high, so that the radial heat conduction through the inter-assembly gap is important for accurate temperature prediction throughout the reactor core. A general liquid flow and solid structure interface model was developed for easier implementation of physics models in the components.
2. Capability to model pool-type reactors. The liquid level tracking, the cover gas dynamics, and the heat transfer between two 0-D components are now implemented. These are important features for accurate SFR safety analysis. For example, the heat transfer from the hot pool to the cold pool would affect the temperatures and liquid levels of the pools, thus significantly affect the natural circulation flow rate in the primary loop and other behaviors during SFR transients.

Some other features were also added to the SFR Module, including the capabilities to model the direct coolant heating and the axial fluid conduction.

3.3 *Multi-Scale Code Coupling*

In additional to the physics and component module development, a multi-scale integration capability is also added to the SFR module to allow coupled code simulations between the system code and other higher fidelity tools.

For practical nuclear engineering applications, multi-scale analysis by adopting the combined use of different scale computational tools, such as system thermal-hydraulics and CFD codes, is vital when three-dimensional effects play an important role in the evolution of a given transient or accident scenario. The feasibility of coupling low-fidelity systems codes with higher fidelity CFD tools was demonstrated previously under NEAMS by coupling SAS4A/SASSYS-1 with the commercial CFD code STAR-CD and STAR-CCM+ [15]. An "ad-hoc" coupling strategy was implemented. The development of new system codes, such as the RELAP-7 code and the SFR module, motivates the development of a coupled scheme for MOOSE-based system analysis codes and the commercial CFD code STAR-CCM+. STAR-CCM+ is a general-purpose commercial CFD code that uses a finite volume formulation for the analysis of compressible and incompressible flows and heat transfer, and it is being included in the toolkit of the NEAMS RPL. This investigation is important for the integration between the MOOSE-based system codes and the high-fidelity advanced simulation capabilities developed under the NEAMS RPL.

Careful control of data exchange flow and the time-synchronization is essential for a numerically stable and physically valid coupled code simulation. The general issues of coupling of system code and CFD code have been addressed in a previous NEAMS report [16], including data exchange method, driving mechanism, time synchronization scheme, and the selection of data for exchange. The coupling strategy between the MOOSE-based system analysis code for SFR and CFD code STAR-CCM+ was derived and implemented based on these considerations and the characteristics of each code. It is briefly discussed here, but the details of the coupling strategy and the implementation can be found in Ref. [16]. The developed strategy for the coupling of MOOSE-based system codes and STAR-CCM+ is also applicable to other multi-scale or multi-physics code coupling applications.

Because STAR-CCM+ is a closed-source commercial code, there are some limitations in what coupling schemes can be implemented. In particular, the iterating two-way coupling scheme, depicted in Figure 2b, is not currently possible to implement since it would require source code modifications of STAR-CCM+ to be able to repeat time steps. Therefore, the sequential two-way coupling scheme depicted in Figure 2a was chosen instead. The MOOSE-based system code is the "master" that starts the calculation of a time step by using the interface information obtained from STAR-CCM+ at the previous time step. Then, the results from the system code at this time step are passed to STAR-CCM+ for its iteration. The time step will be advanced once STAR-CCM+ completes its calculation for the time step.

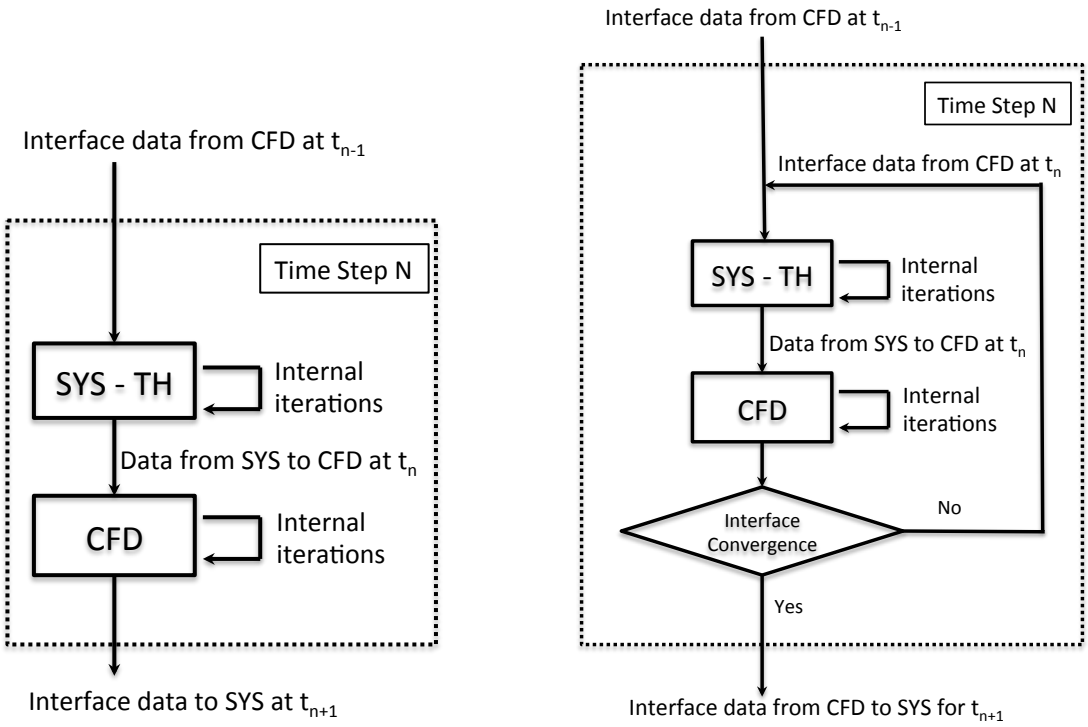

(a) Sequential two-way coupling (b) Iterating two-way coupling

Figure 2: Coupling Schemes for a Generic Time Step

The system code drives the calculation processes as the "master" in the coupled code simulation. A special MOOSE Executioner, CoupledCFDExecutioner, was developed to implement the coupling strategy. The execution process flow is depicted in Figure 3. Before starting the transient calculation, the system code will configure the boundary interfaces for

the coupling, mapping the boundaries defined in the two code models, defining parameters to be received from or sent to the CFD code, in addition to its normal problem configuration and initiation. At each time-step, the system code will read in the CFD simulation results at the coupling boundary interface, complete its own inner iterations for the time-step, and then send out its results at the boundary interfaces to the CFD code for its calculation at this time-step. Once the transient simulation in the system code is completed, it sends out a signal to terminate the CFD code calculation.

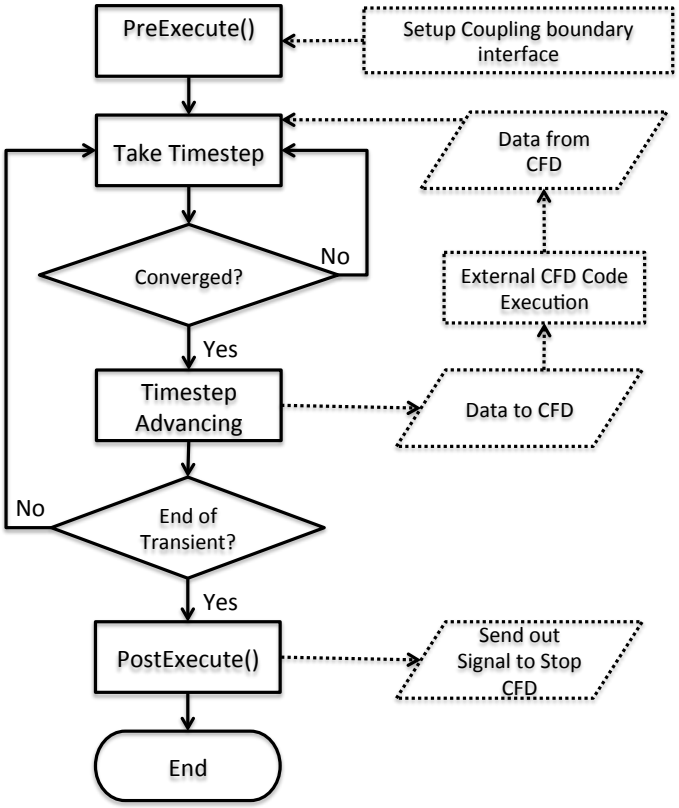

Figure 3: Execution Process Flow Chart of the CoupledCFDExecutioner

The coupling strategy has been demonstrated by several test cases of a simple flow loop model, for which a CFD model of a large tank is coupled to a systems model of the remaining hydraulic pipe loop. Very different system responses were observed during a temperature transient test between the coupled code and the stand-alone system code simulations because the strong thermal stratification in the tank can only be accurately modeled in the coupled code simulation, as seen in Figure 4. The details of the test simulations can be found in Ref. [16]. These preliminary results provided a proof-of-principle of the coupling strategy between the system code and the CFD code, and demonstrated the significance of the coupled multi-scale simulation. In particular, the similar behavior of thermal stratification in the outlet plenum of a SFR would influence the behavior of the primary coolant system in the natural circulation regime.

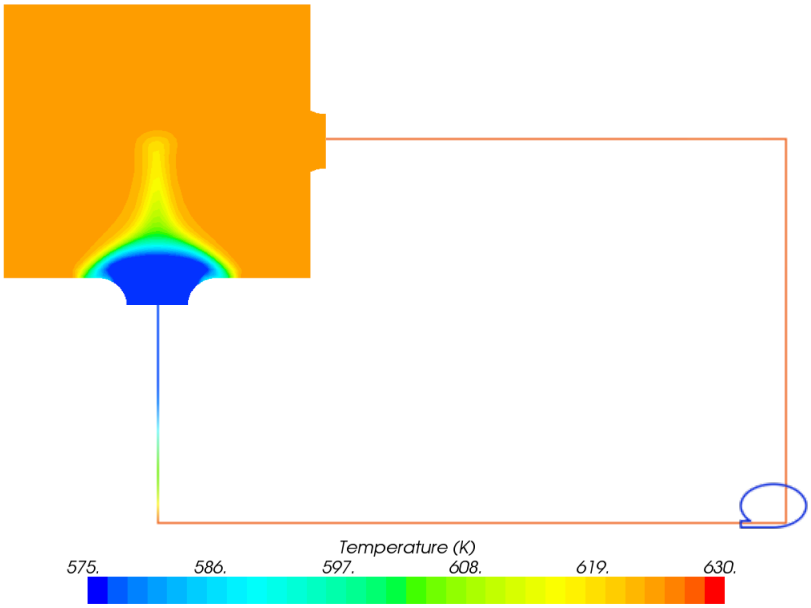

Figure 4: Temperature Distribution in a Coupled System and CFD Transient Simulation

4 SFR Demonstration Simulations with the System Code

A typical SFR system model has been developed to examine the primary system simulation capabilities in the SFR Module. The reactor model is based on the Advanced Burner Test Reactor (ABTR) conceptual design [6]. Both steady state and Protected Loss-Of-Flow (PLOF) transient were simulated. The simulation results were also compared with the SAS4A/SASSYS-1[7] simulation results of the same design.

4.1 *Model Description*

The detailed design parameters of the 250 MW pool type design ABTR can be found in Ref. [6]. The primary system is configured in a pool-type arrangement, with the reactor core, primary pumps, intermediate heat exchangers, and direct reactor auxiliary cooling system heat exchangers all immersed in a pool of sodium coolant within the reactor vessel. The reactor core consists of 24 assemblies in an inner enrichment zone and 30 assemblies in the outer zone. A total of nine test locations are provided for fuel (6 assemblies) and material (3 assemblies) tests. On the basis of the reactor physics calculations, a five-channel model depicted in Figure 5 was selected to model the reactor core. Channels 1 and 3 represent the average subassemblies in the inner and outer enrichment zones respectively, while channel 2 represents the average of the mid-core fuel test assemblies. A fourth channel represents all of the non-fuel subassemblies, including the mid-core materials test assemblies. A fifth channel is used to represent the peak-power inner-core subassembly with fresh fuel. Figure 6 shows the initial subassembly powers at the beginning of equilibrium cycle conditions, and the average axial power shape for all assemblies. The geometric data and input conditions employed in the multi-channel core model are shown in Table 3.

Figure 7 shows the schematics of the ABTR model to be analyzed with the SFR Module. The primary coolant system consists of the Downcomers (pump outlet and pump discharge), the Lower Plenum, the Reactor Core Model, the Upper Plenum, and the intermediate heat exchanger. Five CoreChannels (flow channels with heat structure attached to each of them) were used to describe the reactor core. A Time Dependent Volume component is used to represent the cover gas above the upper plenum. Different components are connected with Branches. The intermediate loop, the secondary loop, and the DRACS loop are modeled with great simplicities. Single-phase counter current heat exchanger models are implemented to mimic the function of the intermediate loop heat exchanger (IHX), DRACS heat exchanger (DHX), and secondary loop heat exchanger (SHX) to transfer heat among the primary, intermediate, secondary, and the DRACS loops. The geometric data of the non-core components employed in the ABTR model are shown in Table 4 and Table 5.

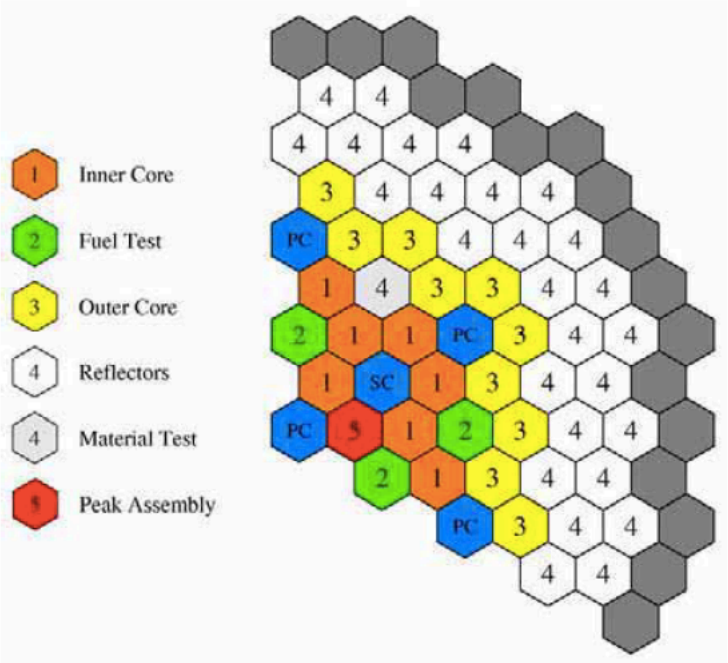

Figure 5: Channel Assignment for Reactor Core [6]

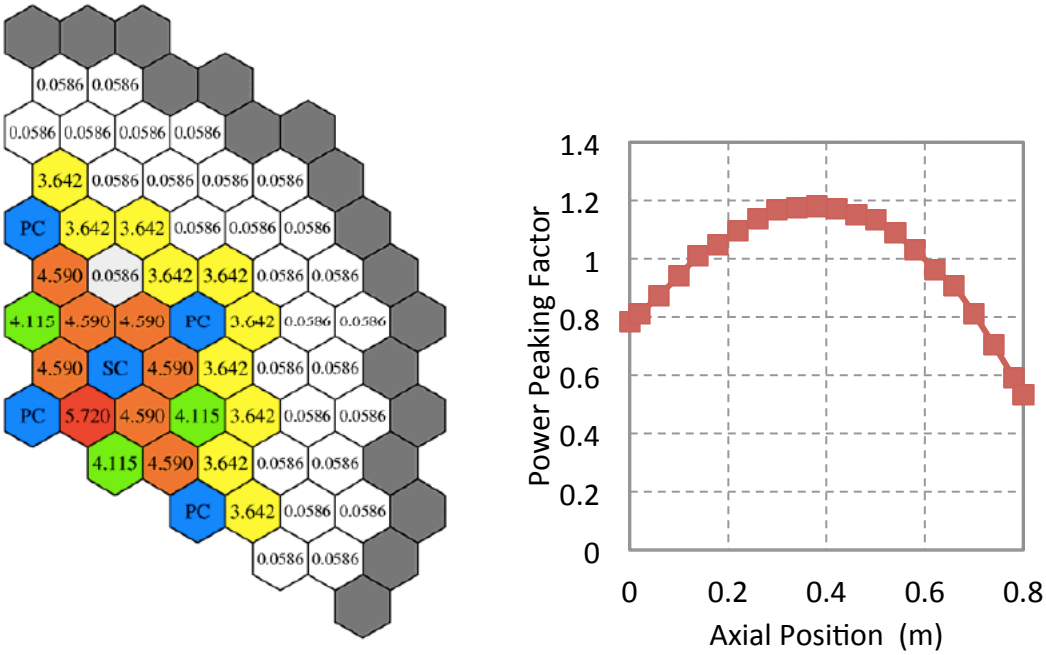

Figure 6: Assembly radial (left) [6] and axial (right) power distribution at BOC

Table 3: Coolant channel model data

	Channel 5	Channel 1	Channel 2	Channel 3	Channel 4
Channel Location	Inner Hot Assembly	Inner Core	Fuel Test	Outer Core	Reflector Channel
Assembly number	1	23	6	30	81
Pin number per assembly	217	217	217	217	91
Power per assembly (MW)	5.62	4.56	4.105	3.59	0.0883
Flow Area (m^2)	0.00492	0.113	0.0295	0.148	0.154
Hydraulic Diameter (mm)	2.972	2.972	2.972	2.972	1.694
Channel Height (m)	0.8	0.8	0.8	0.8	0.8
Fuel pellte radius (mm)	3.48	3.48	3.48	3.48	6.32
Cladding thickness (mm)	0.52	0.52	0.52	0.52	0.70
Inlet Orifice Coefficient	0.5	5.15	5.76	13.2	11100

Table 4: Geometric input data for major out-of-core 1-D components

Component	Type	Inlet Elevation (m)	Flow Area (m^2)	Hydraulic Diameter (m)	Length (m)
Lower Unheated Core	PipeWithHeat-Structure	-0.6	*	*	0.6
Active Core	CoreChannel	0	*	*	0.8
Upper Unheated Core	PipeWithHeat-Structure	0.8	*	*	1.5
IHX Primary Side	HeatExchanger	5.88	0.766	0.0186	3.71
IHX Secondary Side	HeatExchanger	2.17	0.517	0.014	3.71
Pump Pipe	Pipe	3.61	0.132	0.34	4.38
Pump Discharge	Pipe	-0.77	5.36	1	1.26
SHX Primary Side	HeatExchanger	5.88	0.766	0.0186	3.71
SHX Secondary Side	HeatExchanger	2.17	0.517	0.014	3.71
DHX Primary Side	HeatExchanger	6.04	0.024	0.037	2.35
DHX Secondary Side	HeatExchanger	3.69	0.024	0.037	2.35

*: channel dependent, see Table 3.

Table 5: Geometric input data for 0-D volume

Component	Type	Geometric Center (m)	Flow Area (m^2)	Total Volume (m^3)	Ref. Liquid Level (m)
Inlet Plenum	VolumeBranch	-0.77	4.4934	3.06	-
Outlet Plenum	VolumeBranch / LiquidVolume-WithCoverGas	6.45	11.16	92.51	3.59
Cold Pool	VolumeBranch / LiquidVolume-WithCoverGas	2.3	12.8	181.11	4.15

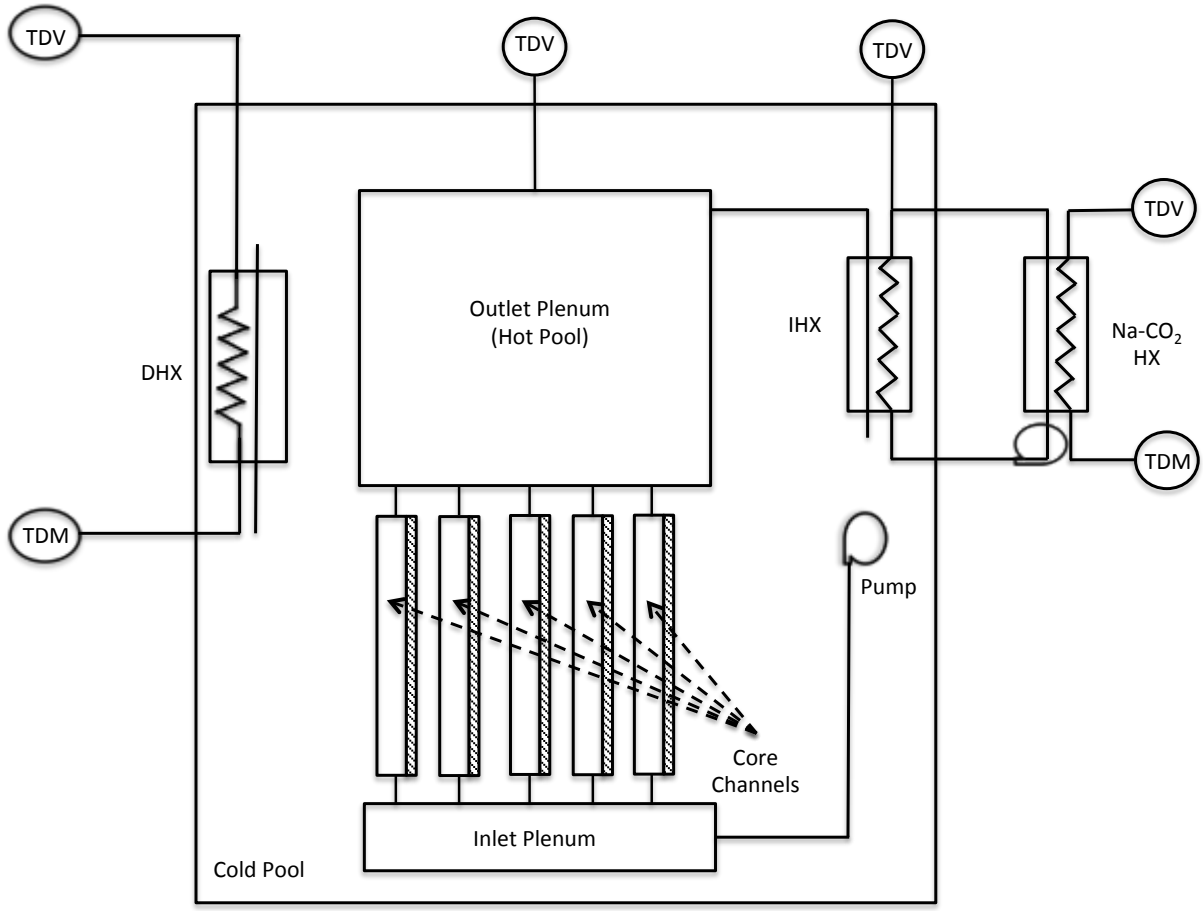

Figure 7: Schematics of the test ABTR model

4.2 *ABTR Steady-State Results*

The steady-state simulation was first performed using the simplified ABTR model described above. Steady state simulation results were obtained via an accelerated time marching transient simulation. Time dependent volumes are applied for the primary and intermediate loops to set up the reference pressure for the two loops. Inlet flow and temperature, and outlet pressure boundary conditions are applied to secondary loop. The flow rate of the DRACS loop was assumed zero for steady-state simulation.

Simulation results were compared with data provided in Ref. [6]. In terms of energy conservation, the core inlet/outlet coolant temperatures provided in Ref. [6] are 628.15 K and 783.15 K, respectively, from which a 155 K core coolant temperature rise can be calculated. The calculated core inlet/outlet temperatures are 627.8 K and 783.9 K, respectively. The calculated core coolant temperature rise is then 156.1 K. This small difference between the simulation and the design data consists of two possible error contributions from mesh discretization (power density discretization) and material properties. In terms of the flow resistance modeling, the calculated primary loop flow rate is 1264.5 kg/s, which is almost identical to the design value of 1264 kg/s. Additionally, the predicted flow rate and temperatures in all heat exchangers agree very well with the ABTR design value, as seen in Table 6. These confirmed that the friction model, form loss coefficients, and the pump head had been consistently set up in the ABTR model. The steady-state SFR simulation capability of the fluid flow and heat transfer can be demonstrated given no flow and temperature boundary conditions were used in the primary and intermediate loop of the test model.

Detailed fluid temperature profiles in the five core channels are shown in Figure 8, including the peak inner subassembly, the average inner subassembly, the average fuel test subassembly, the average outer subassembly, and the average non-fuel subassembly. Different core channel coolant outlet temperatures can be found from the simulation results from different power and flow distributions in those channels. It is interesting to note that the outlet temperature of the non-fuel channel is even higher than the fuel test channel and outer channel. The very high inlet orifice coefficient in the non-fuel channel resulted in a very flow rate and a slightly higher power-to-flow ratio than the fuel test channel and the outer channel. Figure 9 shows the hot core channel axial temperature profiles of coolant, clad surface, and fuel centerline temperatures. The coolant temperature increases continuously as a result of continuous heating from fuel. The fuel center temperature displays a shifted sinusoidal-like shape reflecting the (user input) power density distribution. It is also shown that the temperature differences between the coolant and clad surface are very small, indicating very good heat transfer between the coolant and the HT-9 clad.

The results of inlet velocities and outlet temperatures of the five core channels are compared in Table 7 from both the SFR Module and SAS4A/SASSYS-1 code predictions. Very similar inlet velocities are found for all five channels. The maximum relative difference of the inlet velocities is about 1%, indicating that the flow redistribution among the five core channels is correctly modeled in both codes. However, larger differences in the outlet temperatures are found. The maximum difference of the outlet temperature is 11 K for the hottest core channel. It is also found that the temperature distribution from SAS4A/SASSYS-1 simulation is more flat. This difference will be further investigated.

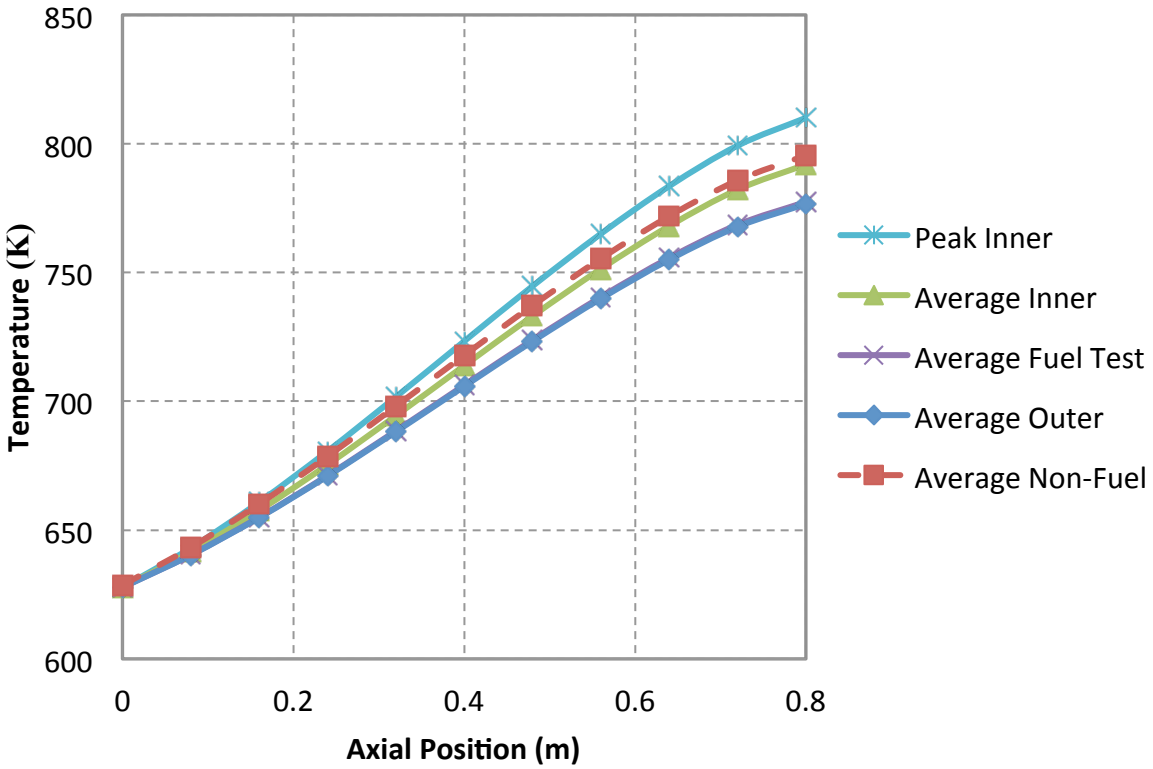

Figure 8: Coolant temperature predictions in five core channels, SFR Module

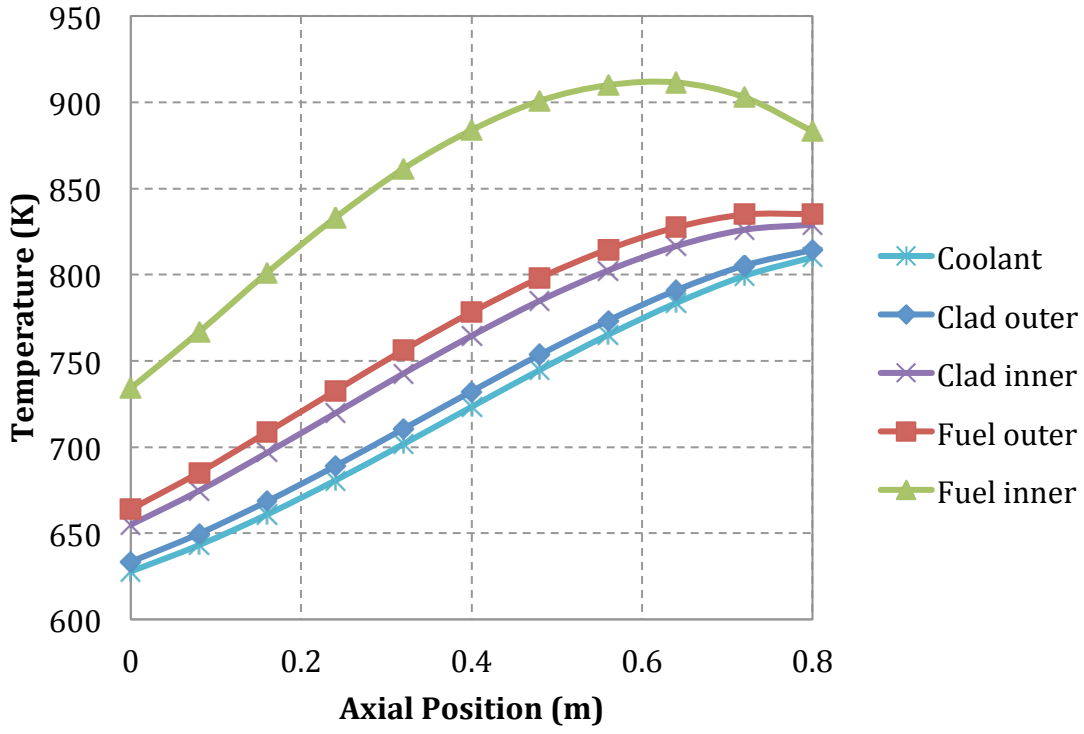

Figure 9: Axial temperature distributions in the hot fuel assembly, SFR Module

Table 6: Comparison of heat exchanger temperature and flow in all loops

	Flow (kg/s)		Inlet Temperature (K)		Outlet Temperature (K)	
	SFR Module	Design	SFR Module	Design	SFR Module	Design
IHX Primary	1264.5	1264	784.0	783.15	628	628.15
IHX Secondary	1259.3	1259	606.5	606.15	762.8	761.15
SHX Primary	1259.3	1259	762.8	761.15	606.5	606.15
SHX Secondary	1259.3	-	596.75	596.75	753.0	-

Table 7: Comparison of inlet velocities and outlet temperature of the five core channels

Core Channels	Inlet Velocity (m/s)			Outlet Temperature (K)		
	SFR Module	SAS4A/ SASSYS-1	Difference (%)	SFR Module	SAS4A/ SASSYS-1	Difference (%)
Peak Inner	5.71	5.65	1.2	810	799	1.4
Average Inner	5.14	5.13	0.32	792	783	1.2
Average Fuel Test	5.08	5.07	0.25	777	784	-0.78
Average Outer	4.47	4.49	-0.44	777	784	-0.89
Average Non-Fuel	0.25	0.25	0.86	795	784	1.52
Mean Difference (%)	0.44			0.48		
Standard Deviation of Differences (%)	0.63			1.20		

4.3 *ABTR PLOF Simulation Results*

4.3.1 Accident Sequences

The basic accident sequence analyzed here is the loss of normal power to the reactor and intermediate coolant pumps, with failure of the emergency power supplies. The result is a loss of forced flow in the primary and intermediate coolant circuits. In addition, it is assumed that heat removal at the power cycle heat exchanger ceases, so that the only heat removal path is through the emergency direct reactor auxiliary cooling system (DRACS). It is assumed that the reactor safety system acts as designed to insert control rods and reduce reactor power immediately to decay heat. This sequence is called the protected loss-of-flow (PLOF) accident.

The natural circulation DRACS consists of heat exchangers located in the cold pool region within the reactor vessel, air dump heat exchangers located outside containment, and the connecting piping. It is simply modeled as a heat exchanger in this demonstration problem. The inlet flow rate, inlet temperature, and outlet pressure are fixed at the secondary side as boundary conditions. The DRACS is designed to remove 0.5% of full power (1250 kW) at normal operating temperatures assuming failure of one DRACS unit.

The initial condition for the accident sequence is normal operation at full power and flow. With the loss of pumping power, flow in the primary circuit coasts down according to the spinning inertia of the pumps and motors. Following flow coast down, natural circulation flow is established. With the loss of power, forced flow in the intermediate coolant system is also lost. Further, it is assumed that heat rejection through the power cycle heat exchanger ceases. The intermediate heat transport system (IHTS) is alternately a heat sink or source in the accident sequence, depending on its temperature and the primary system temperature at the intermediate heat exchanger. During the transient, flow in the IHTS may reverse, depending on transient temperature conditions.

In the PLOF sequence, the absence of normal shutdown heat removal through the reactor coolant system causes a slow system temperature rise following the reactor scram. This temperature increase occurs because the DRACS has insufficient heat removal capacity to overcome both the early decay heat production rate and the stored heat in the primary and intermediate systems. Eventually, the decay heat falls below the DRACS capacity, and the system temperature declines.

4.3.2 SFR Module Simulation Results

At this time, the detailed reactivity feedback mechanism, decay heat, and the pump models have not been developed in the SFR Module. Therefore, the reactor power and primary pump head history from SAS4A/SASSYS-1 simulation results, shown in Figure 10, were used throughout the simulated PLOF transient. The pump in the intermediate loop is assumed to have the same coast-down characteristics. Both pumps were assumed to completely stop at about 420s.

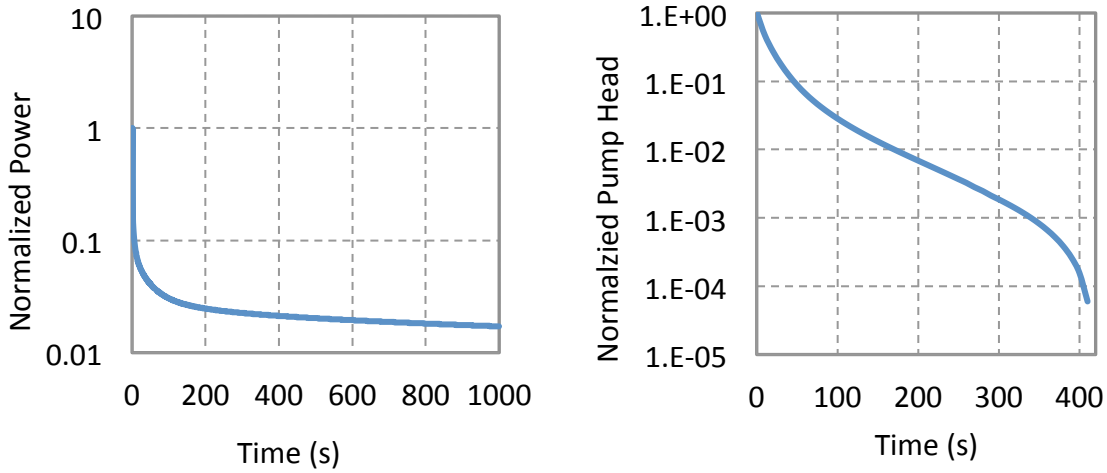

Figure 10: Normalized power and pump head history during PLOF

Results from analysis of the earlier PLOF transient during the pump coast down and transition to natural circulation are shown in Figure 11-Figure 16. The normalized core power and flow rate are shown in Figure 11. This transient is initiated by a complete loss of forced coolant flow in the primary and intermediate loops. Both the primary and intermediate pumps are designed with sufficient flow inertia, and cease operation at about 420 seconds after the start of the transient, leading to a transition to natural circulation. Immediately after the transient initiated, the reactor control system scrams the reactor, and then the reactor power is shortly reduced to decay heat. It is found in Figure 11 that the transition to natural circulation

flow is very smooth. The power to flow ratio during the transient is actually always less than that of normal operating conditions, which assures that the safety of the reactor core during the transient. Figure 12 shows the flow velocities in all core channels during the transient. Similar behaviors are found, and the establishments of the natural circulation flows occur at the same time for all channels.

Figure 13 shows the DRACS heat removal and the IHX heat removal rates. When the transient is initiated, the secondary side of the DRACS heat exchanger is assumed open immediately, permitting the DRACS to operate at its full capacity of removing 0.5% nominal power. As the cold pool temperature rises, DRACS heat removal capacity will increase accordingly. The loss of heat removal to the balance-of-plan is also assumed immediately after the transient by setting the flow in the secondary side of the secondary heat exchanger to zero. It is also shown in Figure 13 that the heat removal rate from DHX is far less than the reactor decay heat power at the end of 1000 seconds. The DRACS heat removal capacity will equal the decay heat at about 5 hours into the transient. A close view of the heat removal rate from IHX is shown in Figure 14. In spite of the very simplified model of the intermediate loop, it behaves alternately as a heat sink or source during the transient, depending on its temperature and the primary system temperature at the intermediate heat exchanger. This behavior is expected in the ABTR IHTS design.

The temperatures at the core inlet plenum, outlet plenum, and the cold pool are shown in Figure 15, and the maximum temperatures in the core are shown in Figure 16. Shortly after the transient, the only heat removal is through the DRACS. The rapid reactor power decrease due to the scram initially lowers the coolant and fuel rod temperatures in the core, and then the hot pool temperature. Then the drop in core flow due to the pump coast down and the increase of the core inlet temperature leads to the temperature rise in core and the hot pool. The cold pool temperature rises during the whole transient because the hot coolant continues entering the cold pool from the IHX outlet, and the heat removal from the DHX is not enough. This will continue until the DRACS heat removal capability becomes equal to the decay heat production, which will occur at about 5 hours. After that, the cold pool temperature will decrease as the whole system cools.

This demonstration simulation focuses on the early stage of the PLOF transient. It is confirmed that major physics phenomena in the primary coolant loop during the transient can be captured by the SFR Module simulation.

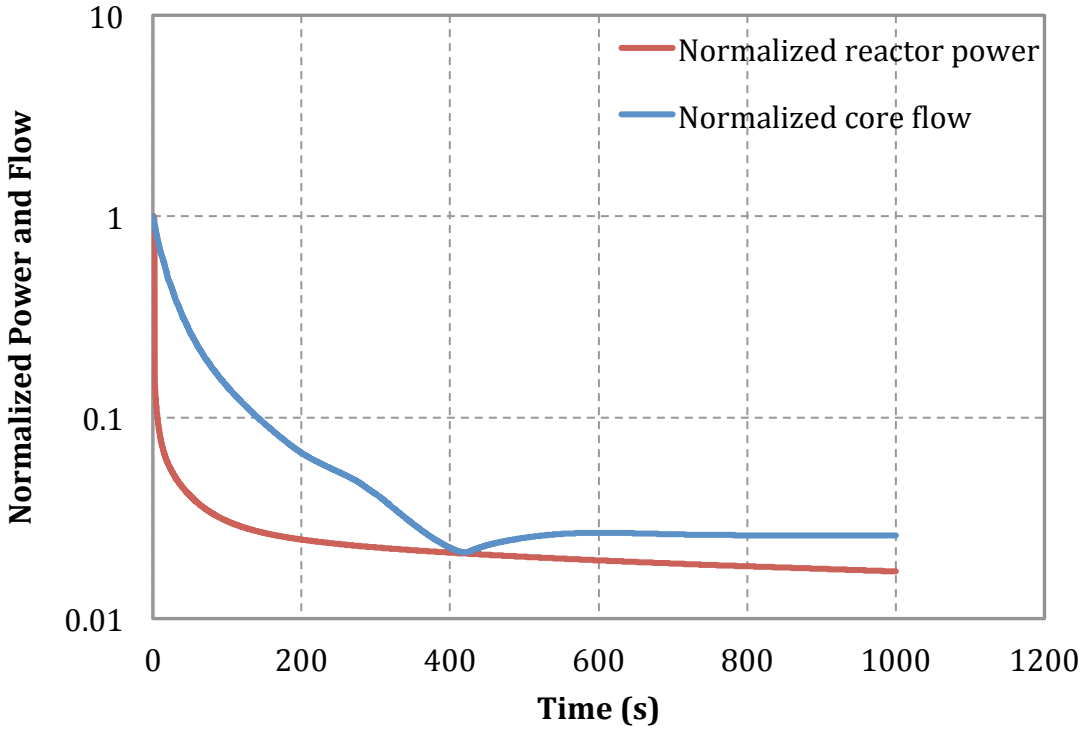

Figure 11: Normalized power and core flow during the PLOF transient

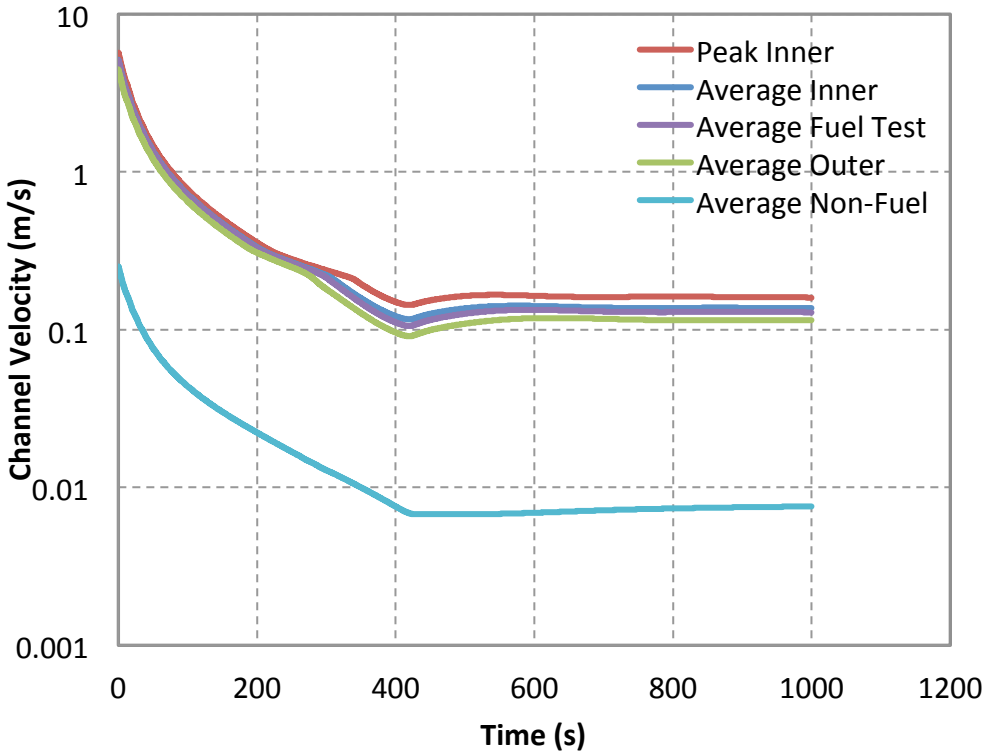

Figure 12: Core channel flow velocities during the PLOF transient

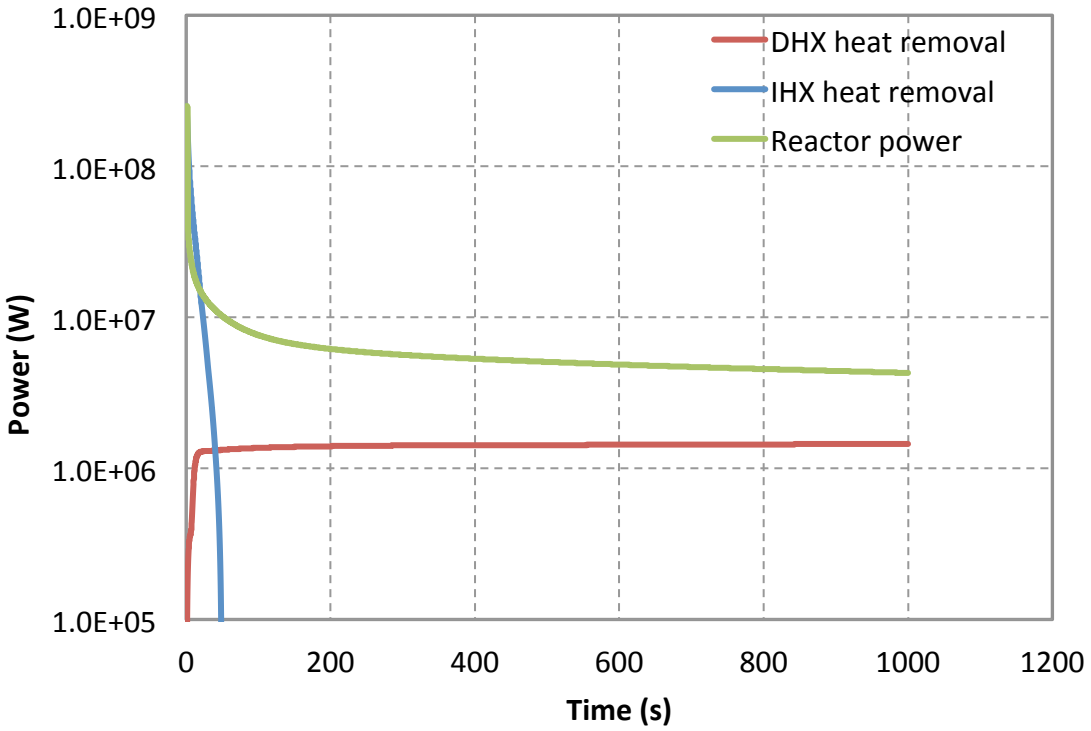

Figure 13: Heat removal rate during the PLOF transient

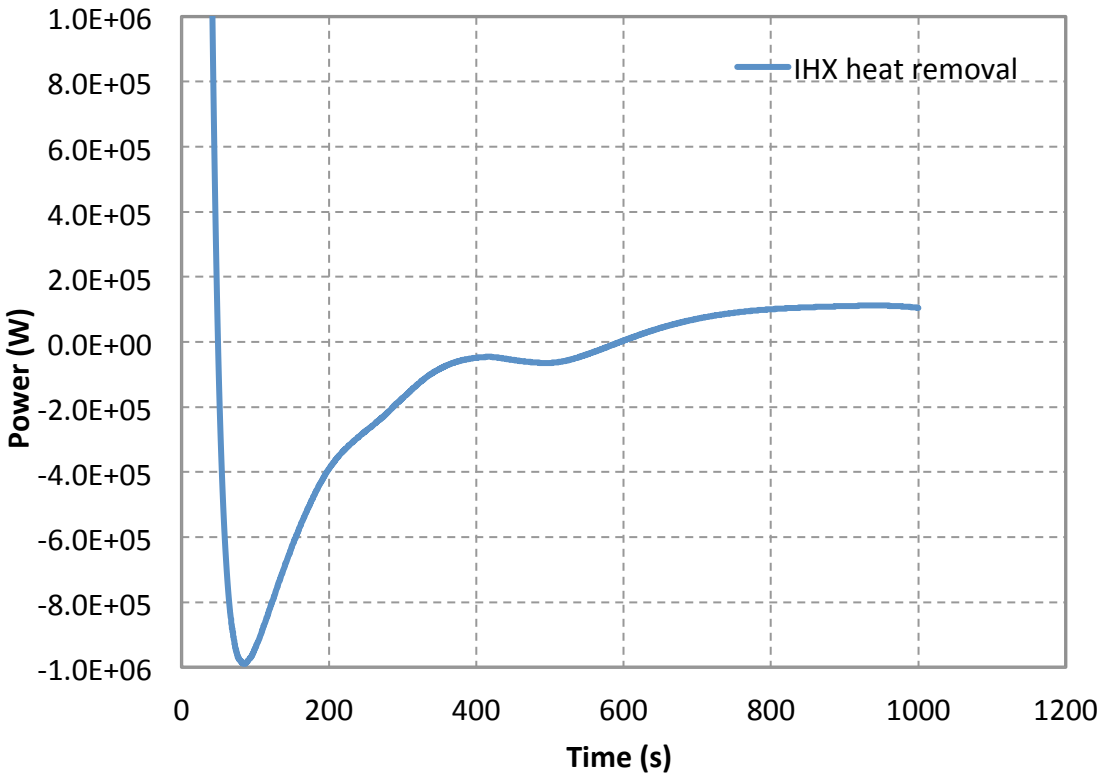

Figure 14: Heat removal rate from IHX during the PLOF transient

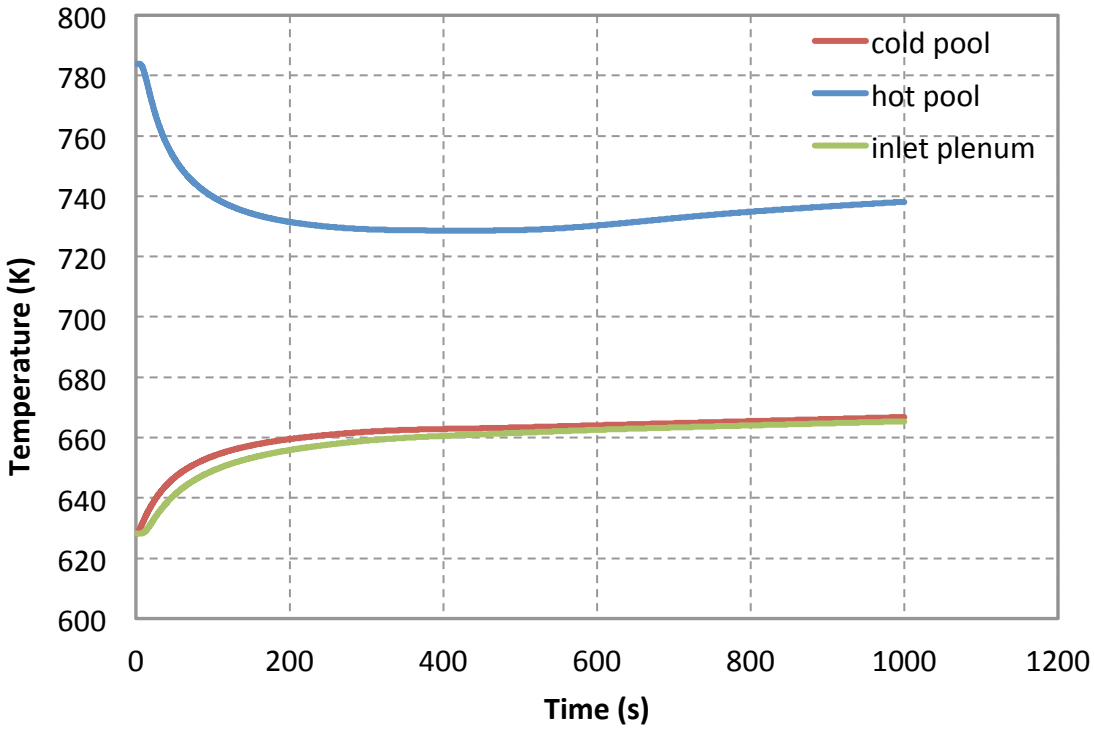

Figure 15: Pool temperatures during the PLOF transient

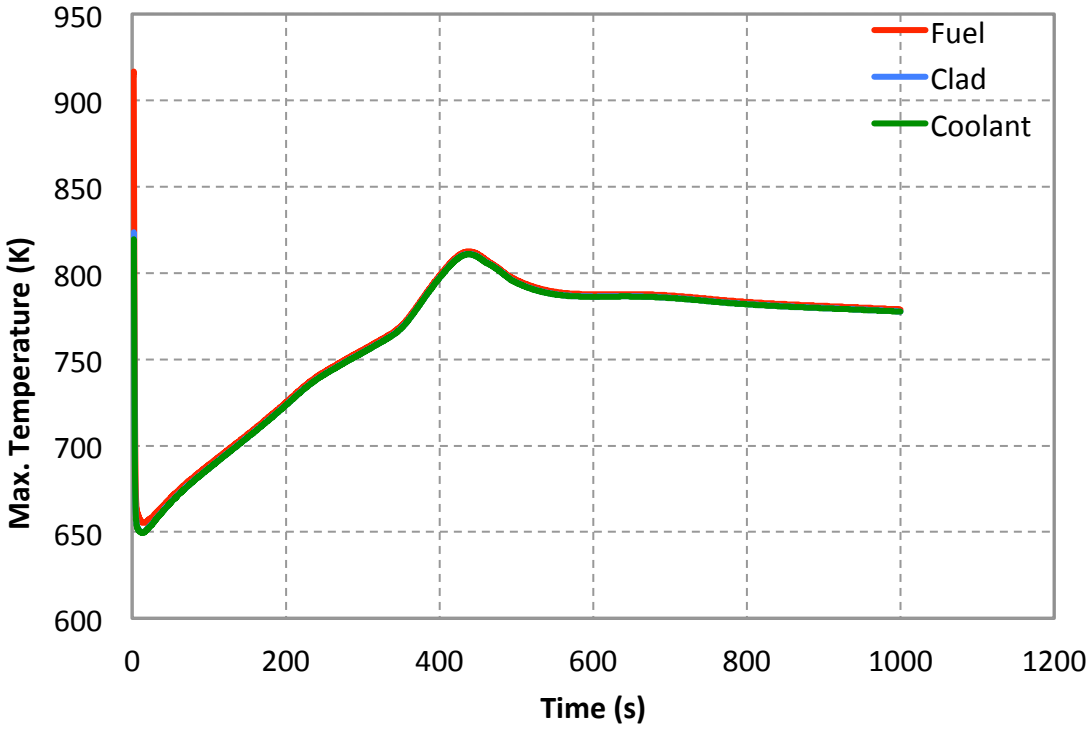

Figure 16: Core maximum temperatures during the PLOF transient

4.3.3 SAS4A/SASSYS-1 Results

The SAS4A/SASSYS-1 model developed for ABTR safety evaluation [6] was used in this work for a code-to-code benchmark. Major results from the SAS4A/SASSYS-1 simulation of the earlier PLOF transient are shown in Figure 17 - Figure 20 during the pump coast down and transition to natural circulation. Although the overall system behavior is similar between the SFR Module and the SAS4A/SASSYS-1 simulations, the magnitude of the temperature peaks or flow troughs are quite different.

Among all the modeling differences between the two code simulations, the most important one is the differences in modeling the cold pool. A temperature stratification model for the cold pool is used in the SAS4A/SASSYS-1 simulation, while the current SFR Module does not have this capability and a perfect mixing model is used for the cold pool. Additionally, the heat transfer between the hot and cold pools through the redan wall is included in the stratified cold pool model in SAS4A/SASSYS-1; this effect is also neglected in the base model of the SFR Module.

In SAS4A/SASSYS-1 simulation, the hot coolant entering the cold pool from the IHX outlets rises to the upper part of the cold pool, forming a hot layer. The cooler discharge from the DRACS heat exchangers falls to the bottom of the cold pool, forming a cold layer. The temperature stratification effect in the cold pool is indicated by the temperatures plotted in Figure 18. For most of the transient the temperature in the upper stratified layer of the cold pool is approximately equal to the hot pool temperature; whereas the temperature in the lower layer is approximately equal to the inlet plenum temperature. This temperature difference is approximately 100°C. Note that the “Cold Pool” temperature plotted in the figure is the average temperature of the axially stratified distribution.

The average cold pool temperature in SAS4A/SASSYS-1 simulation is much higher than that of the SFR Module, as seen in Figure 19, which reduces the driving head and thus hurts the establishment of the natural circulation flow. This explains the lower prediction of core flow rate after the loss of forced flow, as seen in Figure 17. The lower prediction in core flow rate leads the higher prediction of the core temperature in Figure 20 since the reactor power is the same in the two simulations. It is also interesting to find that the inlet plenum temperature is initially much lower than the average cold pool temperature in the SAS4A/SASSYS-1 simulation due to the stratification. After 500 seconds, the interface between the hot and cold layer in the cold pool drops low enough so that the pump intake starts receiving hot fluid from the upper hot layer. Therefore, a fast increase of inlet plenum temperature is seen in Figure 18 and Figure 19, and it eventually surpass the average cold pool temperature at about 900 seconds. In the SFR Module simulation, the inlet plenum temperature is always similar to the average cold pool temperature since the cold pool stratification is not modeled.

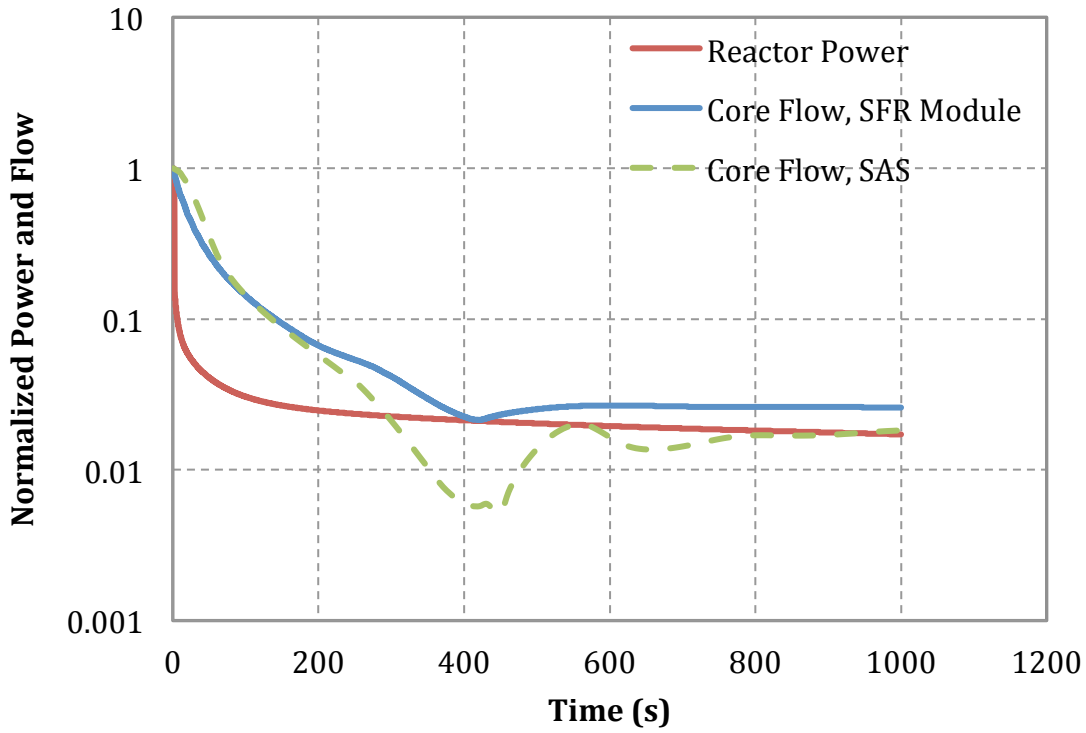

Figure 17: Normalized power and flow during PLOF, SAS and SFR Module results

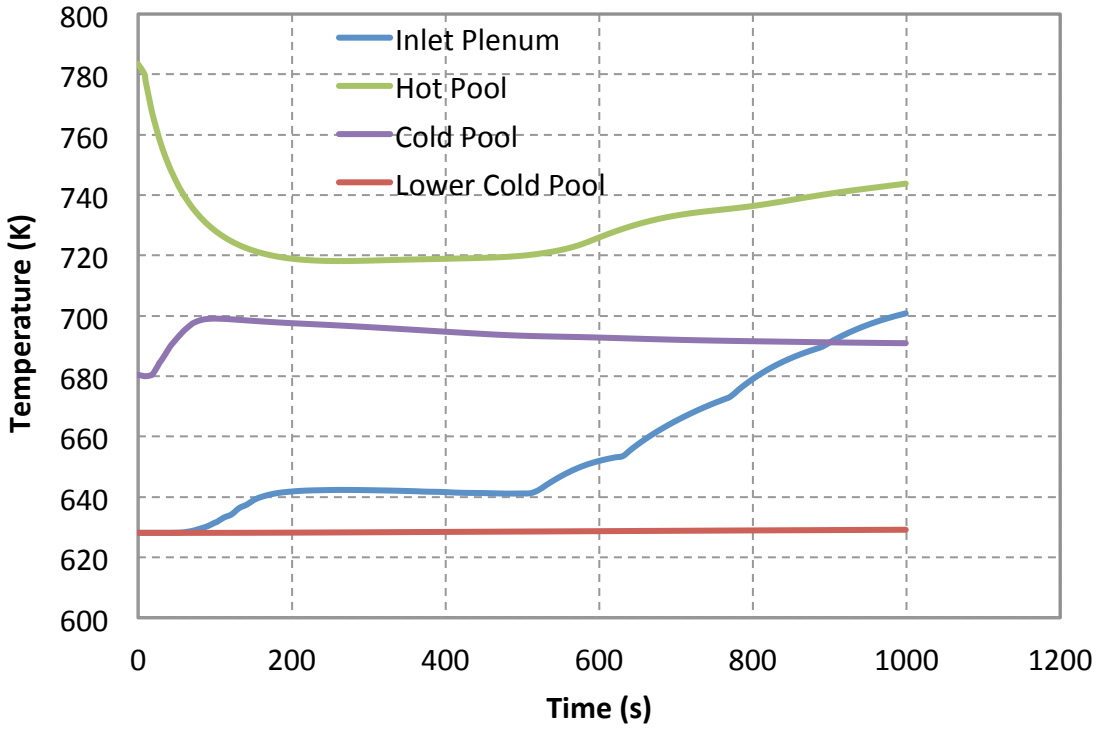

Figure 18: Pool temperatures during the PLOF transient, SAS results

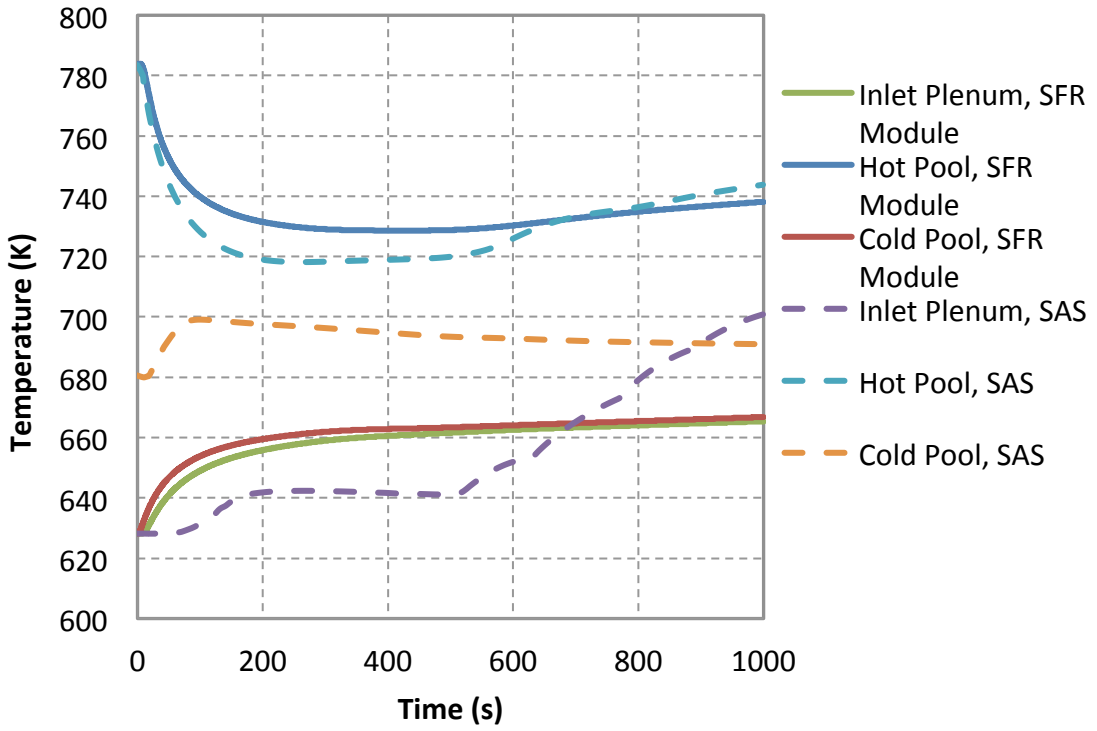

Figure 19: Pool temperatures during PLOF, SAS and SFR Module results

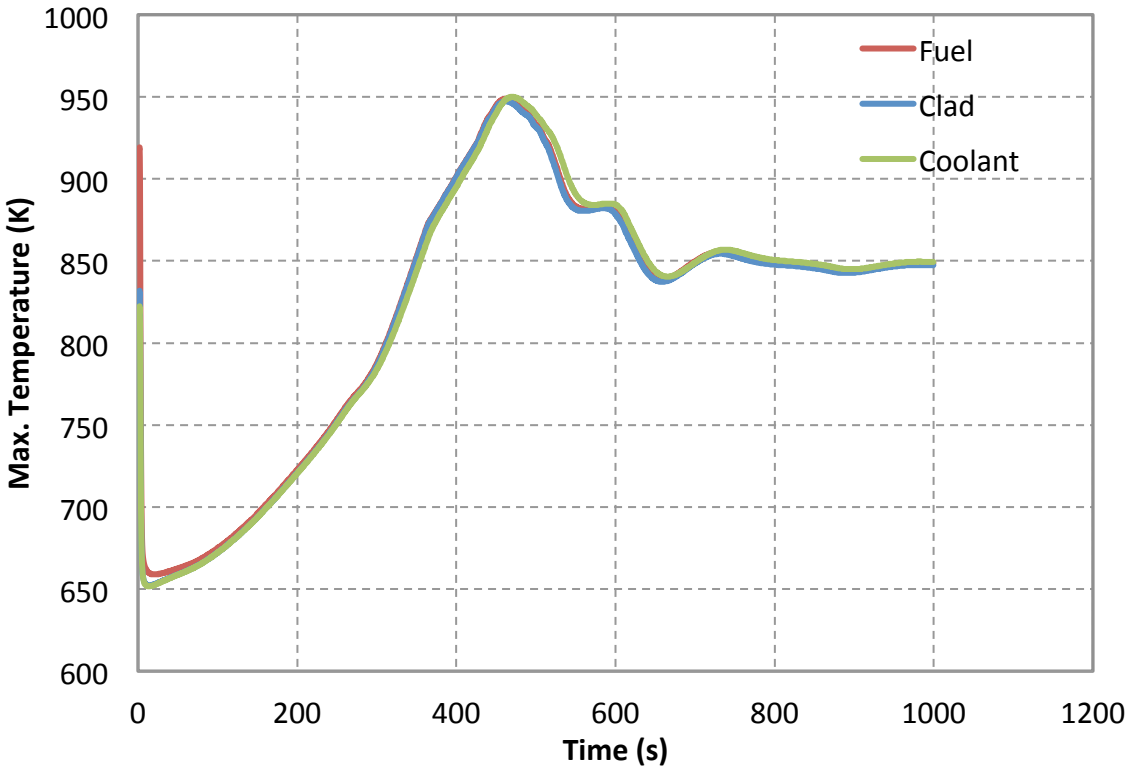

Figure 20: Core maximum temperatures during the PLOF transient, SAS results

To examine the effects of the stratified cold pool model, another SAS4A/SASSYS-1 simulation was performed with a perfect mixing model used for the cold pool. The predicted core flow and pool temperatures are compared with other simulations in Figure 21 and Figure 22. With the perfect mixing cold pool model, the SAS4A/SASSYS-1 results are similar to those of SFR Module, and the establishment of the natural circulation flow is smoother than the stratified model. However, the long term natural circulation flow is lower than the SFR Module predictions. This could be due to the differences in the friction models used in the two codes, and in the cold pool modeling. It is still not clear why the inlet plenum temperature is very different from the cold pool temperature in the simulation of SAS mixed cold pool model.

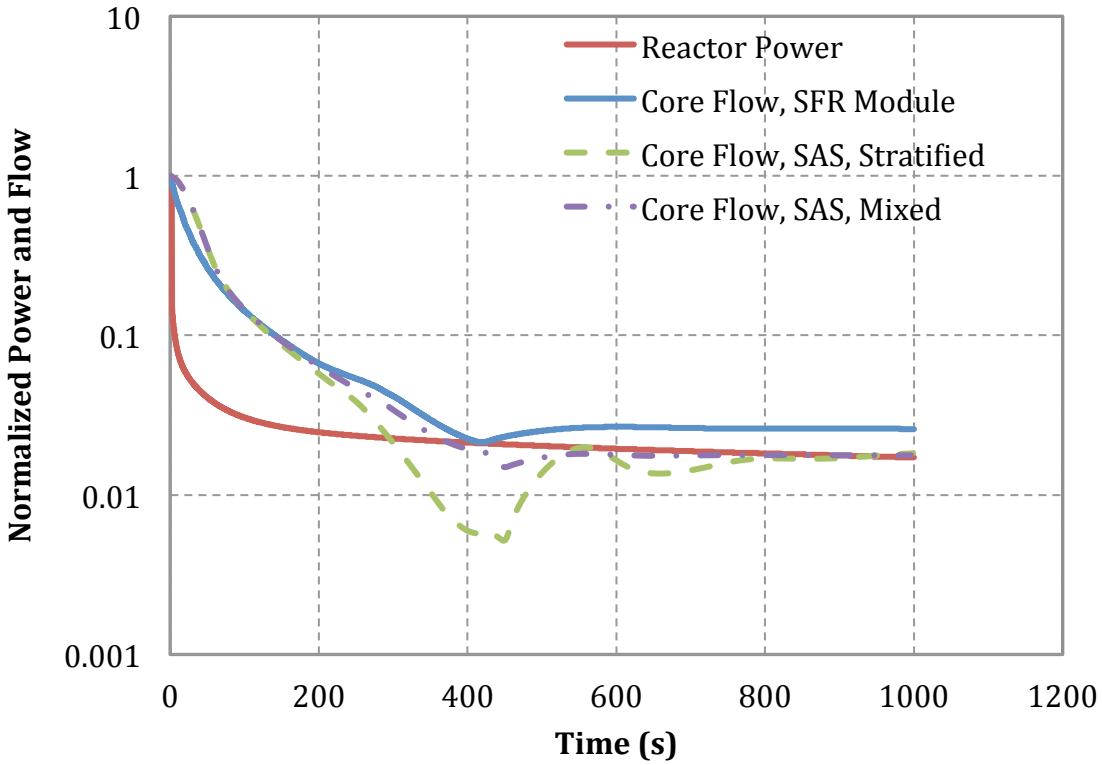

Figure 21: Normalized power and flow during PLOF, effects of stratified model

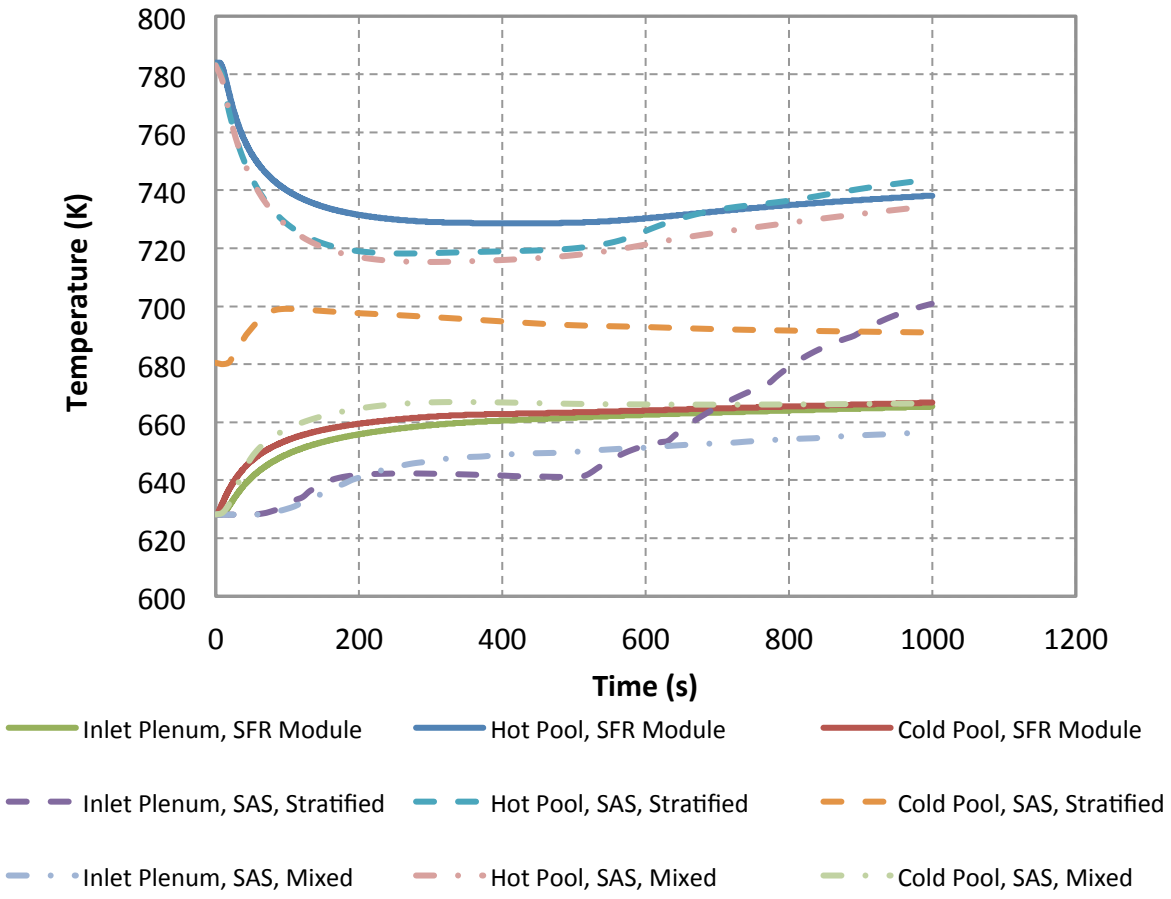

Figure 22: Pool temperatures during PLOF, effects of stratified model

4.3.4 Effects of the Heat Transfer between the Hot and Cold Pools

To examine the effects of the heat transfer between the hot and cold pools, another SFR Module simulation was performed with a redan wall modeled between the two pools. Convection heat transfer between the redan wall and the two pools, and the heat conduction inside the redan wall were then captured in this simulation. The cold pool is modeled as two liquid volumes, with the upper one connected to the redan wall and the cover gas and lower one connected to the pump inlet and IHX outlet.

The predicted core flow and pool temperatures are compared with the base case simulation in Figure 23 and Figure 24. The core flow rates in the two simulations are nearly the same during the transient. It indicates that the heat transfer between the hot and cold pools through the redan wall has insignificant effects to the natural circulation flow rate. However, the pool temperature predictions are quite different. If the wall heat conduction is considered, the upper cold pool temperature is close to the hot pool temperature, and the lower cold pool temperature is also higher than the average cold pool temperature in the base case, during the whole transient. This in turn increases the core inlet temperature and the maximum coolant, clad, and fuel temperature in the transient.

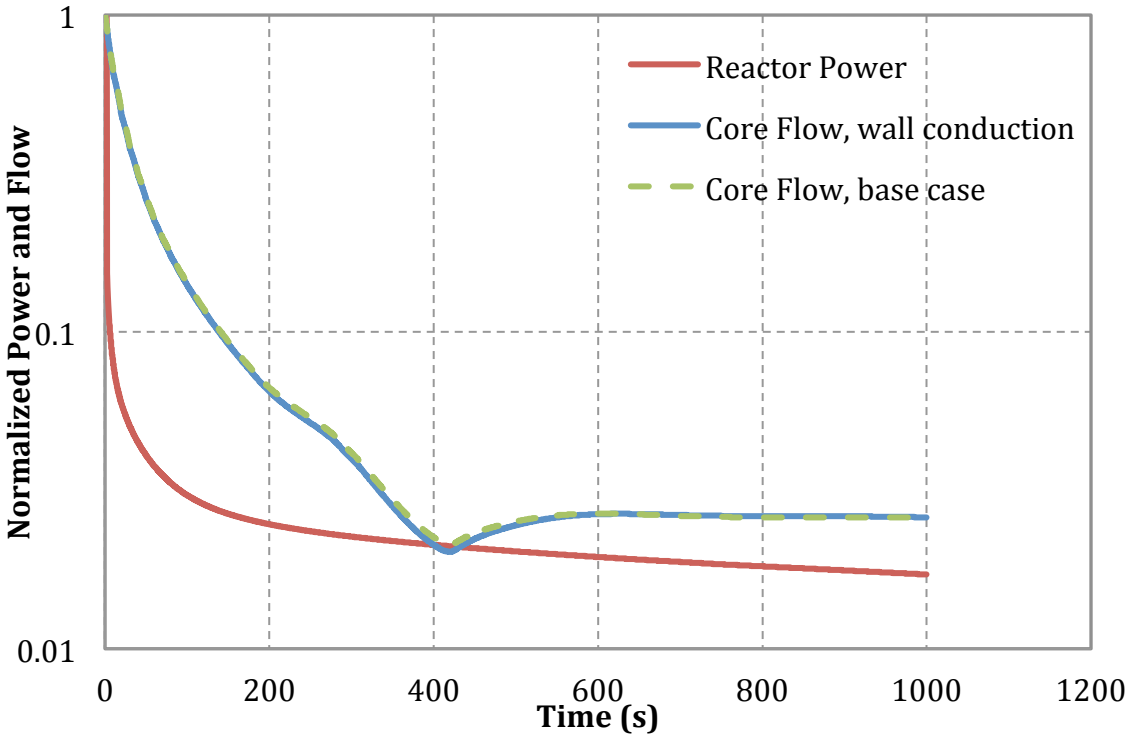

Figure 23: Normalized power and flow during PLOF, effects of redan wall conduction

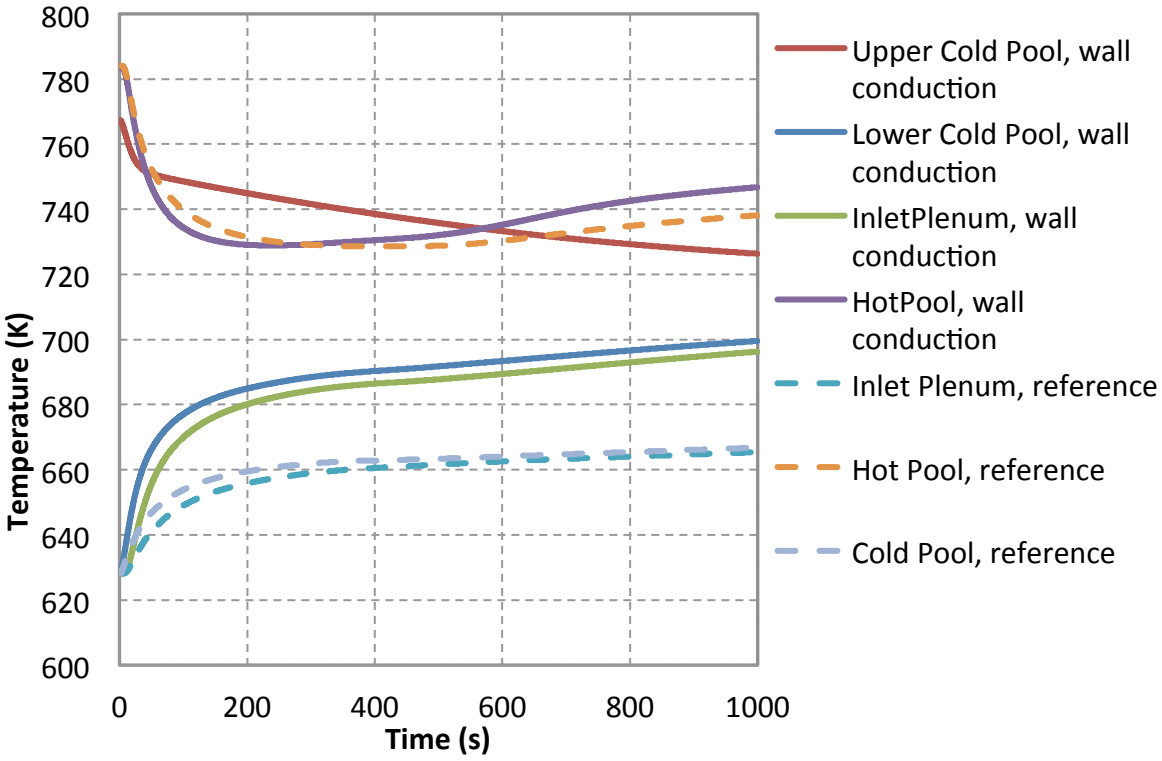

Figure 24: Pool temperatures during PLOF, effects of redan wall conduction

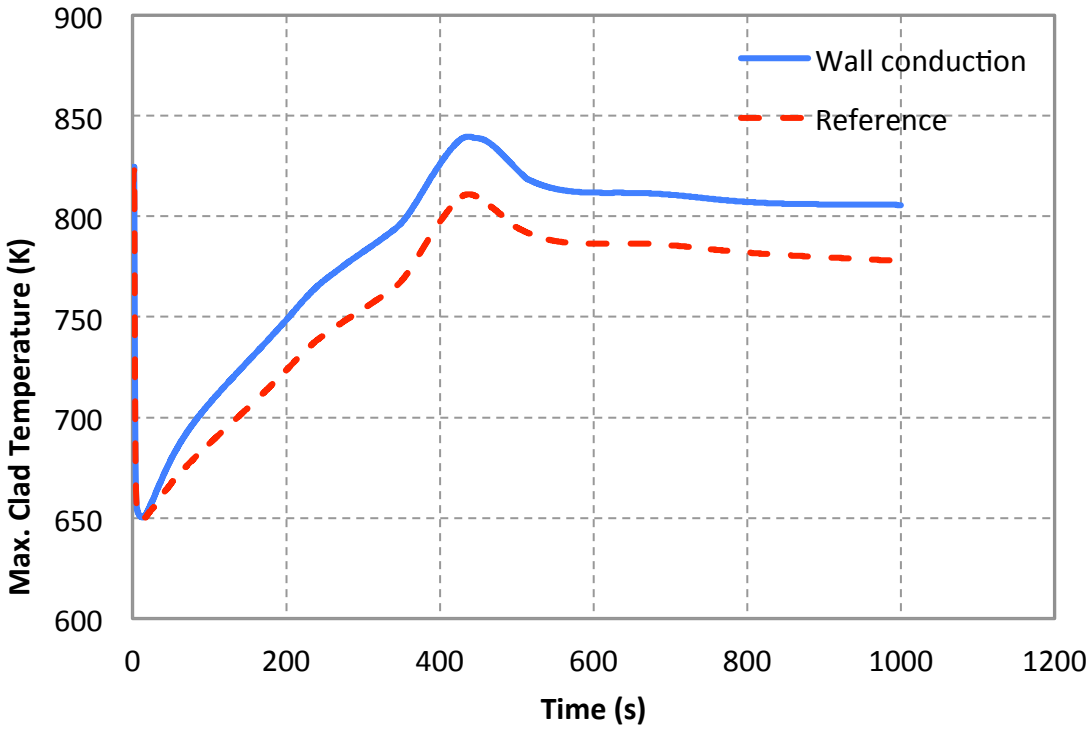

Figure 25: Maximum clad temperatures during the PLOF transient, effects of redan wall conduction

5 Coupled System and CFD Code Simulation of ABTR PLOF

The coupling strategy between the SFR Module and STAR-CCM+ has been developed and demonstrated in the previous work [16] by a simple test model as a proof-of-principle. In the protected loss of flow transient of a pool type sodium fast reactor, it is expected that the multi-dimension effects in the cold pool and hot pool, and the formation of thermal stratification layers will play an important role in the evolution of the accident. Therefore, the coupled code system is examined again to simulate the PLOF transient of ABTR. Although the stratification in the cold pool is also important to the transient behavior, as confirmed in Section 4.3.3, this study focused first on the multi-dimension effects in the hot pool. In the future, both the hot and cold pools will be modeled by the CFD code in a coupled multi-scale simulation of the PLOF.

To perform the coupled code simulation of transients, the stand-alone simulations of both codes have to be conducted first to approach the desired initial states prior to the transient. This is followed by a null transient simulation with the coupled code to assure the consistency at the boundary interfaces before initiating the transients.

5.1 *Model Description*

In the coupled code simulation of ABTR PLOF, the core outlet plenum is modeled by STAR-CCM+, while the rest of the system is modeled by the SFR Module. Therefore, the outlet plenum in Figure 7 is replaced by three boundary interfaces (CoupledTDVs) in the coupled model, as depicted in Figure 26. For initialization at the nominal operating condition, fixed pressure and temperature boundary conditions are used for these CoupledTDVs in the stand-alone system code simulation.

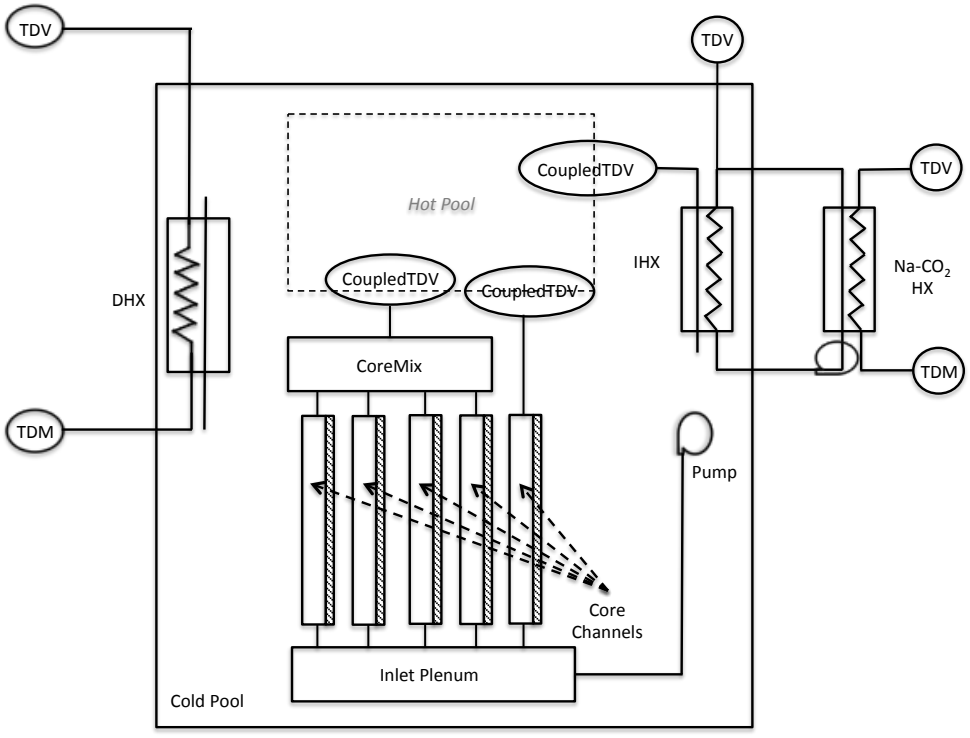

Figure 26: ABTR model in the coupled code simulation

The CFD model solves the transport equations for mass, momentum, and thermal energy of the ABTR upper plenum. The implicit unsteady model is employed to predict time-sensitive conditions using a stable solver. The tank coolant includes both the primary sodium coolant and cover gas. The two phases are modeled using the volume-of-fluid approach, which is applicable for modeling immiscible fluids where the two phases may be approximated to share a common velocity, pressure, and temperature field. In this case, including a model of the cover gas allows the level of the sodium/gas interface to move during the transient, thus providing the necessary compressibility to permit the system code to specify the flow rate at all flow boundaries. The temperature dependence of the sodium density, thermal conductivity, and molecular viscosity is treated using the same polynomials available in SAS4A/SASSYS-1. The cover gas is argon, which is treated as an ideal gas. Turbulence is modeled using the SST k-ω model with all-y+ wall treatment. The SST k-ω model is one of several Reynolds-Averaged Navier Stokes (RANS) models available in STAR-CCM+ and has been chosen over the Realizable k-ε model because improved convergence properties for this particular model.

The geometry of the ABTR hot pool is inferred from its Preconceptual Design Report [6]. The model includes the coolant confined by the redan wall, but outside the core, IHX and associated piping, upper core structure (UCS or UIS), fuel handling machine, and other structures. The core barrel, IHX, and upper internal structure are subtracted from the coolant inside the redan. The core and barrel are approximated as a single cylinder, subtracted from the hot pool region. The upper core structure is approximated as a rounded cylinder with no flow inside. The fuel handling machine and other miscellaneous structures are omitted from this model. The secondary-side IHX piping and kidney-shaped IHX vessel are represented. Symmetry is assumed, such that only a quarter of the hot pool is modeled. The resulting geometry is shown in Figure 27, with the values of the geometric parameters in Table 8.

The main body of the ABTR hot pool is a cylinder with height and diameter of 12 m and 3.48 m, respectively. The two IHXs are positioned in kidney-shaped regions on opposite sides of this region. At the initial (i.e. nominal operating) condition, the outlet of the core and reflector subassemblies serve as the inlet to the hot pool, and the inlet to the IHX serves as its outlet. In the actual ABTR core design, there are many hexagonal subassemblies arranged in a lattice. The arrangement of the core outlet is simplified substantially in this model. The hot central fuel subassemblies are grouped together and approximated as a circle, labeled “Core Inlet” in Figure 27. The reflector subassemblies surrounding the core are represented as an annulus, labeled “Ref Inlet”, just outside the core. The model assumes zero flow through the shielding subassemblies—which is consistent with the system code model—and thus the annulus outside the reflector is a wall boundary. The IHX inlet boundary is modeled as a 0.2 m high rectangular window facing the core barrel, as can be seen in the inset in Figure 27. This differs from the description in the Preconceptual Design Report, which specifies several 0.2 m diameter circular holes, but does not describe the number or position of these holes. In the absence of detailed specifications, the rectangular window was chosen for its simplicity. The edges of the inlet, the upper core structure, and the IHX walls were rounded to avoid sharp gradients and even reversed flows in those regions.

The reference mesh has a total of 4.2 million cells and is depicted in Figure 28. The trimmer mesher was employed for the internal mesh, which generates hexahedral cells except where cells are “trimmed” at boundary surfaces. The hexahedral cells are oriented such that

each cell has a pair of faces orthogonal to each coordinate direction. Thus cells in the vicinity of the liquid/gas interface have 2 pairs of faces normal to the interface. A base mesh size of 0.02 m was employed with 10 layers of prismatic cells along the walls. In the vicinity of walls with relatively high-speed flow—including the IHX walls, upper core structure, and portions of the redan wall—the number of prism layers was increased to 15 in order to reduce y+. The areas surrounding the inlets and outlet were refined to improve the convergence of turbulence transport equations, especially in the vicinity of the bottom of the upper internal structure where substantial turbulence is generated as jet traverses the curved surface.

Velocity inlet boundary conditions are applied to all flow boundaries. At a velocity inlet boundary, a specification of both temperature and velocity must be provided, along with turbulent intensity, turbulent viscosity ratio, and the volume fractions of the liquid and gas phases. Despite the name, it is not necessary to provide inward-directed flow at an inlet boundary, and in fact outward-directed flow is specified for the IHX window. In the case of outward-directed flow, the solvers ignore the specified values of the temperature, turbulence, and volume fraction. For initialization at the nominal operating condition, fixed uniform velocity and temperature profiles were assigned to the inlet boundaries. The velocity and temperature boundary conditions for the core inlet are 1.34 m/s and 783.62 K and 0.027 m/s and 795.34 K for the reflector. At the IHX window, the specified velocity is -3.76 m/s. The negative sign is to denote outward flow boundary.

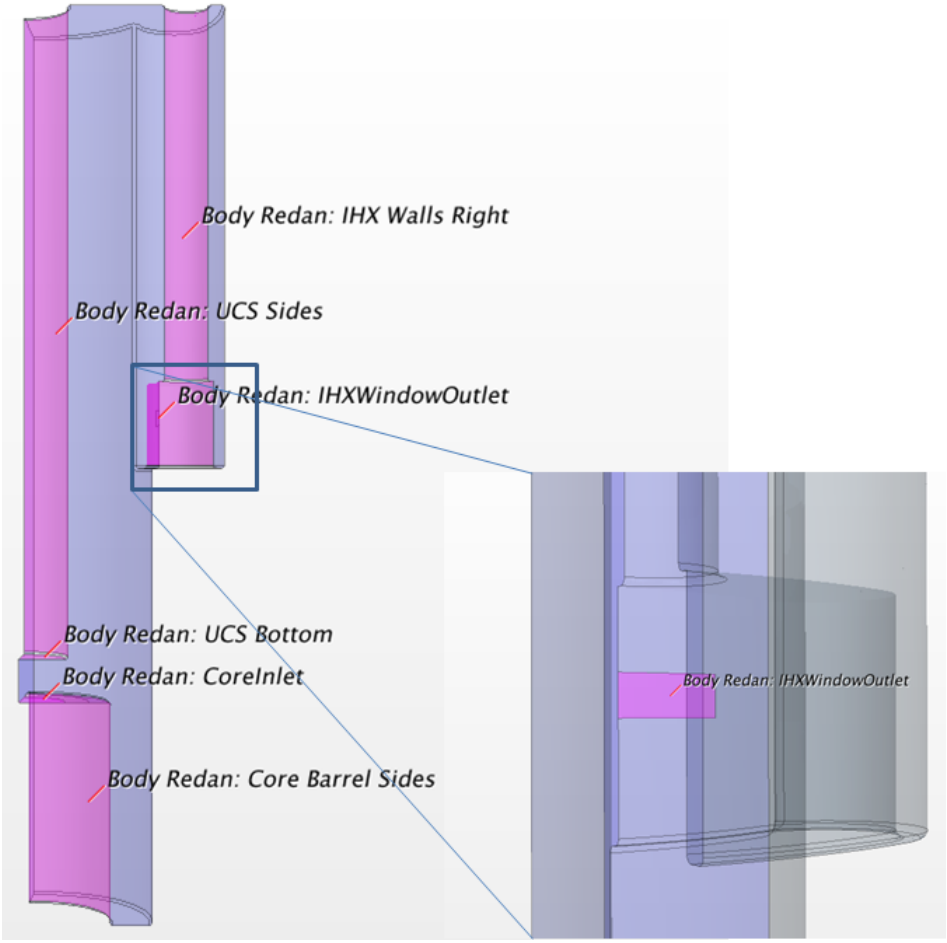

Figure 27: Front View of the ABTR Upper Plenum Geometry in STAR-CCM+

Table 8: Geometry of the Upper Plenum Model in STAR-CCM+

Parameter	Description	Value (m)
D_{redan}	Inner diameter of the redan	3.48
D_{ref}	Outer diameter of the reflector inlet	1.82
D_{core}	Outer diameter of the core inlet	1.188
H_{redan}	Height of the redan	12
z_{in}	Elevation of the inlet centerline, relative to the bottom of the redan	2.95
z_{out}	Elevation of the IHX outlet centerline, relative to the bottom of the redan	6.626

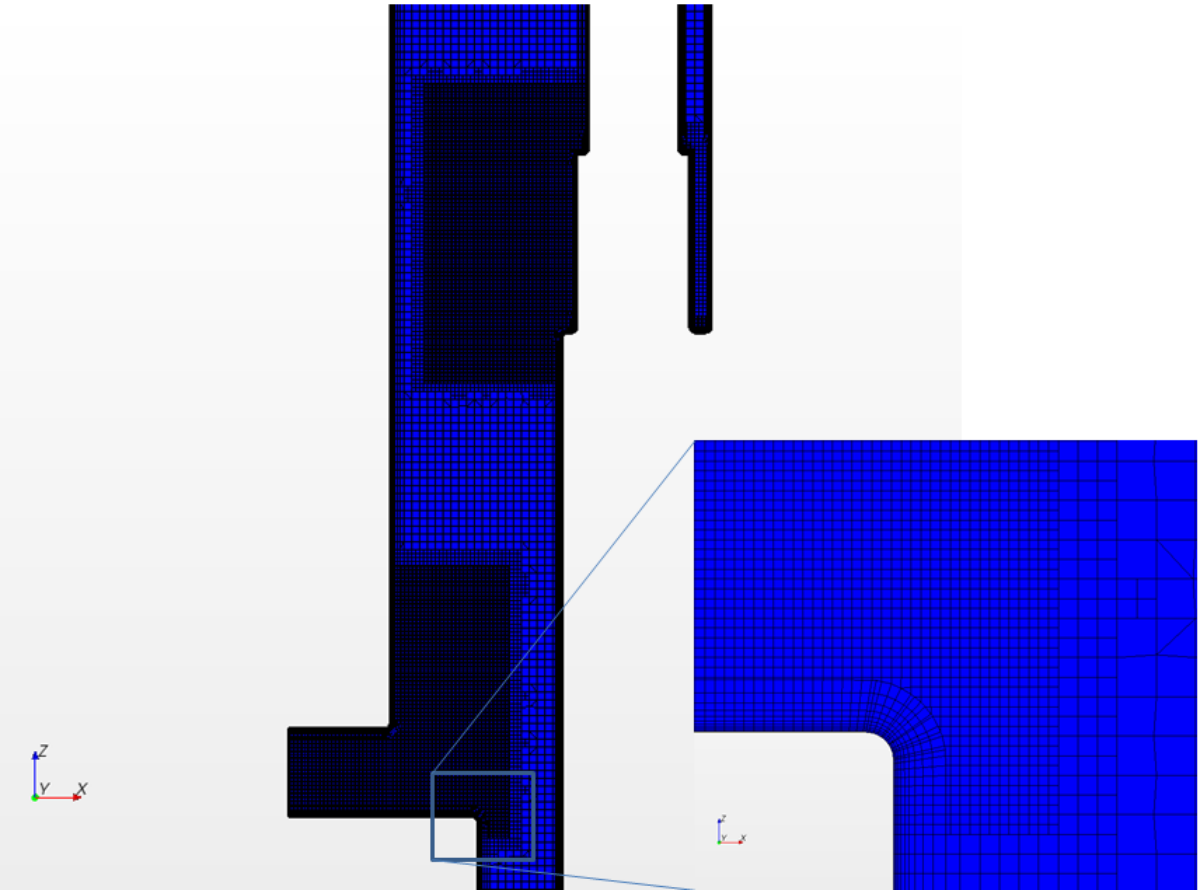

Figure 28: CFD Mesh in the Vicinity of the Inlet and Outlet Boundary Surfaces

5.2 *CFD Model Initialization*

In order to initialize the coupled code calculation, a standalone STAR-CCM+ calculation was performed with boundary conditions consistent with the coupled calculation at t=0. This calculation employed the unsteady solvers with fixed boundary conditions and 0.01 s time steps. The simulation was run off-line for more than 1 minute in an effort to achieve equilibrium. In fact, a significantly longer time would be required to achieve an equilibrium temperature profile. Given that the difference in the initial temperature between the core and

reflector outlets is only 6K, the conditions achieved after 1 minute were deemed suitable for the purposes of this demonstration calculation.

The velocity field evolved from a condition with zero velocity to the equilibrium condition that features a jet dissipating into the redan, accelerated flow near the UCS bottom and the outlet junction, and recirculation in the region far from both flow boundaries (see Figure 29). From Figure 30, the liquid/gas interface is relatively flat, but does expand in the center slightly due to the influence of the jet. The interface is diffused across 3 mesh cells, a distance of 0.06 m, due to mesh resolution and numerical diffusion. The sharpness of the interface should be improved in future work, but the interface dynamics are not important to the current demonstration problem. The absolute pressure field is provided in Figure 32. The pressure profile exhibits a relatively uniform gradient, as gravity is the primary influence. The initial temperature in the tank was set to 783K, approximately the mass flowrate-weighted average of the two inlet temperatures. Although the temperature in the upper plenum as shown in Figure 31 is fairly uniform initially, a major thermal stratification phenomenon is predicted during transient analysis.

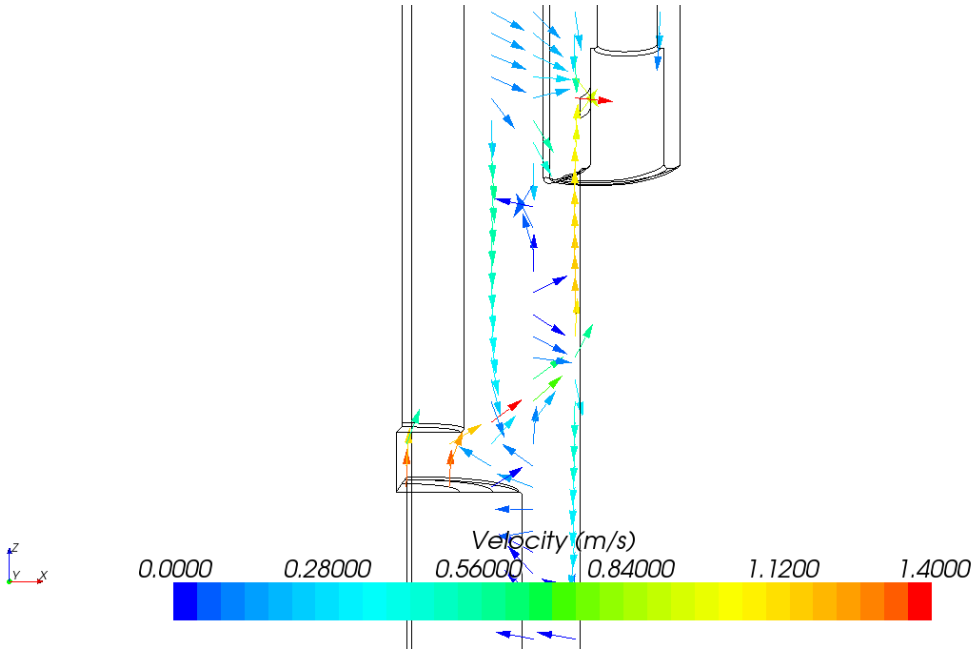

Figure 29: CFD Prediction for the Velocity Field at the Initial Condition at the Vertical Plane Slicing through the Centers of the Inlet and Outlet Boundary Surfaces

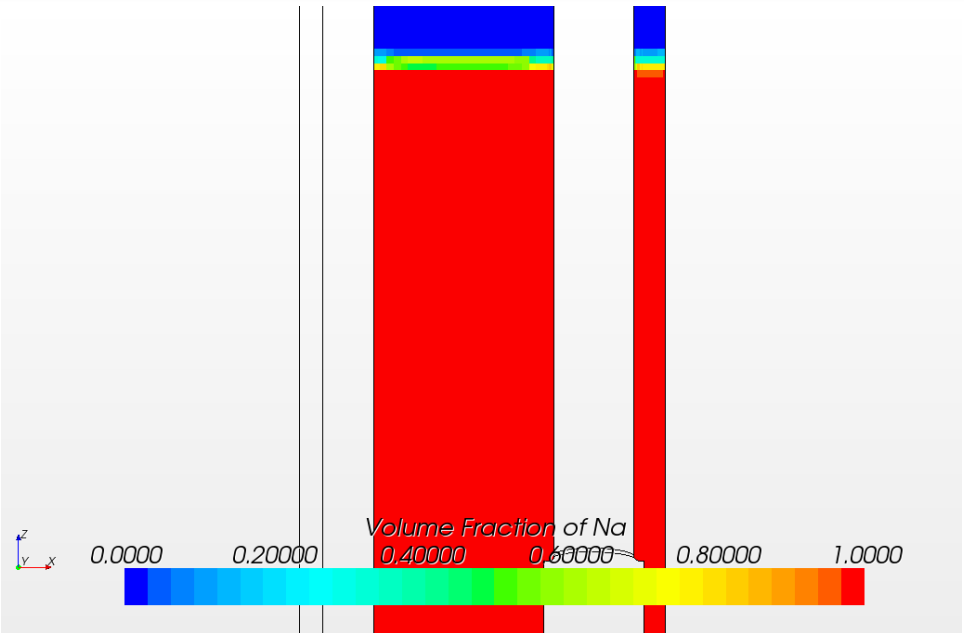

Figure 30: CFD Prediction for the Sodium Volume Fraction at the Initial Condition at the Vertical Plane Slicing through the Centers of the Inlet and Outlet Boundary Surfaces

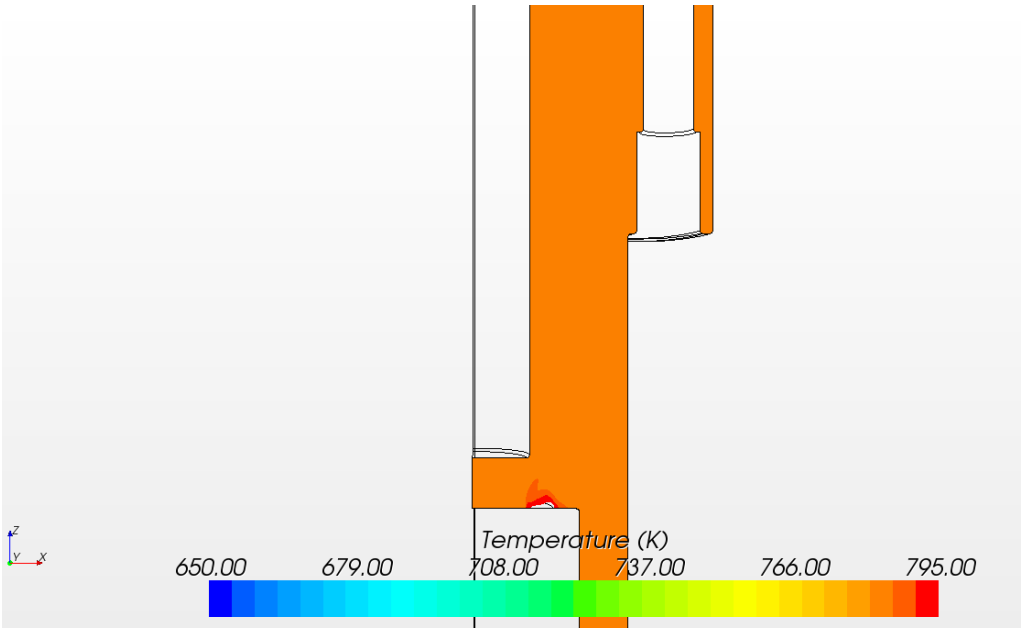

Figure 31: CFD Prediction for the Temperature at the Initial Condition at the Vertical Plane Slicing through the Centers of the Inlet and Outlet Boundary Surfaces

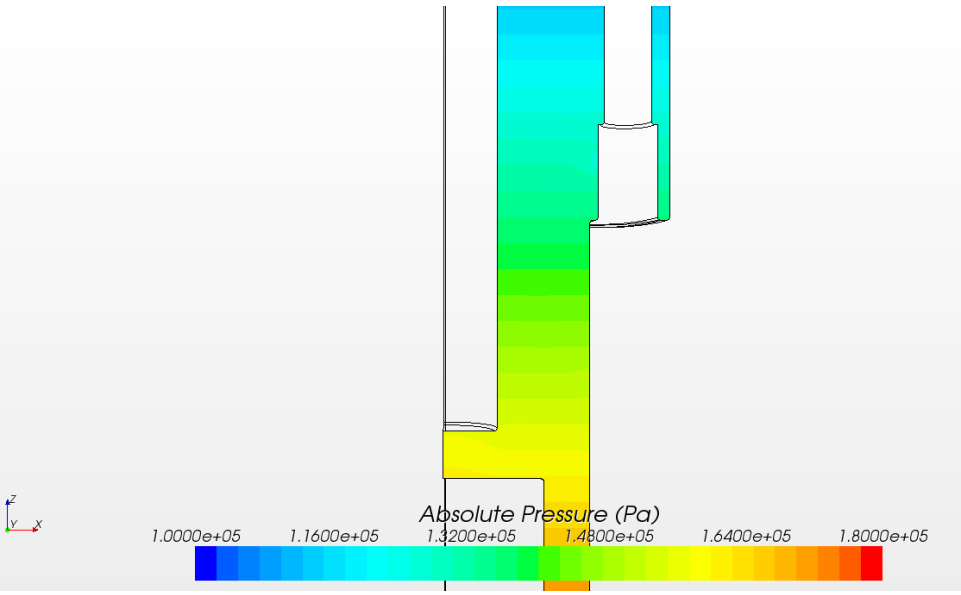

Figure 32: CFD Prediction of the Pressure at the Initial Condition at the Vertical Plane Slicing through the Centers of the Inlet and Outlet Boundary Surfaces

5.3 *Sensitivity Study on Time Step Size*

5.3.1 Standalone CFD simulation

A study was performed to investigate the time step size effects in CFD for the coupled calculation. Standalone CFD simulations were first performed using time-dependent boundary conditions determined by the standalone system code simulation of the ABTR PLOF. These boundary conditions are shown in Figure 33 and Figure 34. The first 50 seconds of the transient simulation were performed with three time step sizes: 0.005 s, 0.01 s, and 0.05 s. This time period covers much of the flow coastdown and the sharp decrease in core outlet temperature in response to scram. The flow from the core and reflector outlets are always directed into ("In" in Figure 33) the hot pool and the flow through the IHX is always directed out ("Out" in Figure 33) of the hot pool. Since the temperature at outward-directed boundaries does not need to be specified, the IHX boundary temperature is not provided in Figure 34.

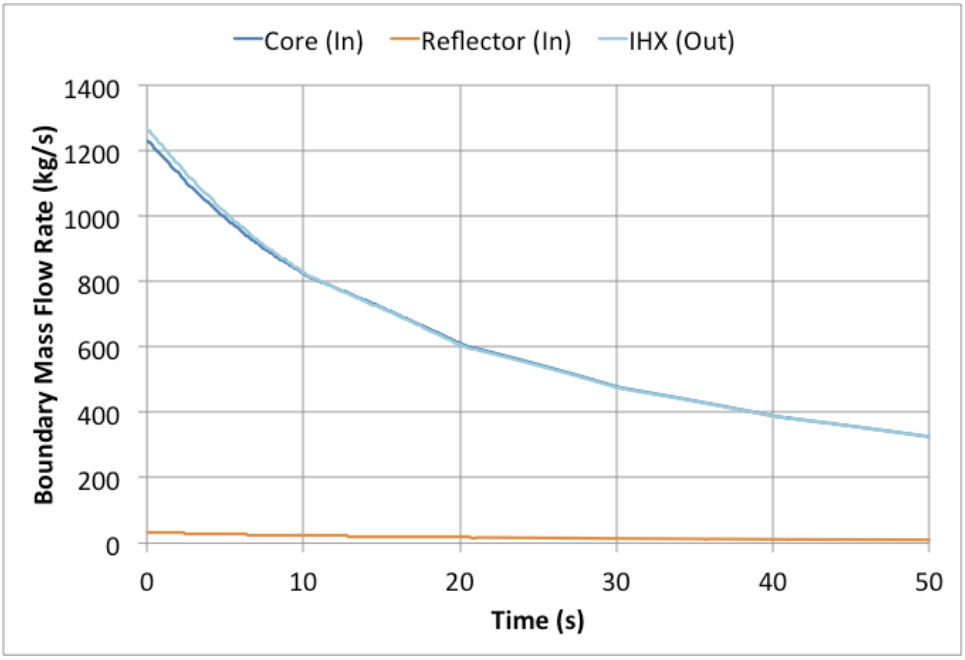

Figure 33: Flow Rate Boundary Condition in CFD Time Step Size Study

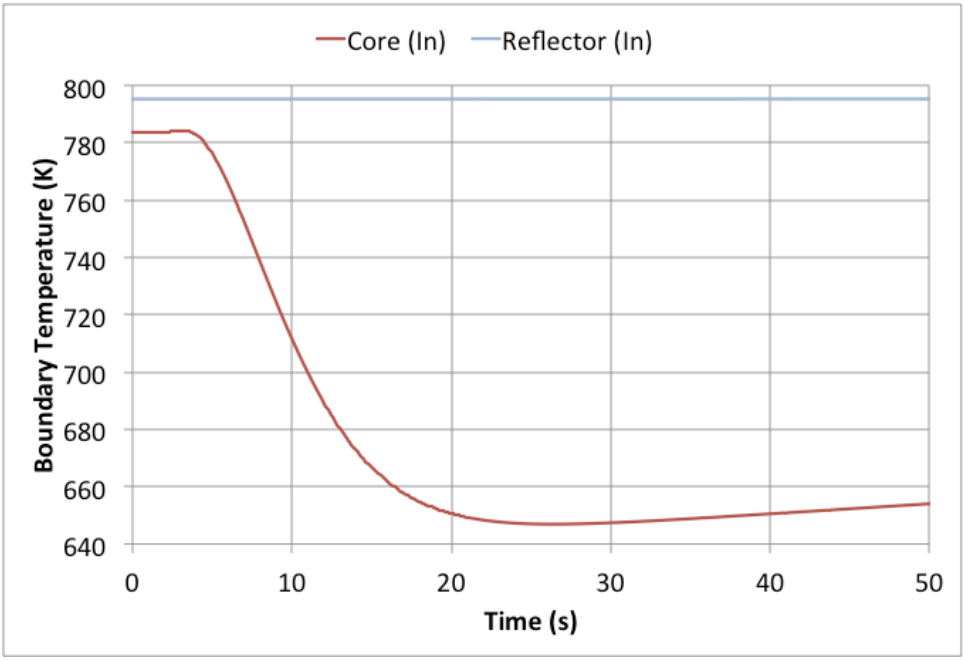

Figure 34: Temperature Boundary Condition in CFD Time Step Size Study

The predicted evolutions of the IHX inlet temperature and the difference in pressure between the core and IHX boundaries are plotted in Figure 35 and Figure 36. These quantities are of particular interest, because they will be transferred to the system code during coupled calculations. The trends in the IHX boundary temperature are significantly different after 45 seconds, perhaps indicating different flow topologies. It is thus confirmed that the flow dynamics in the upper plenum during the transient is sensitive to the time step size used in the analysis. Further investigation would be required to better understand the discrepancy or

improve the CFD model. For accurate CFD simulation results, smaller time step should be selected.

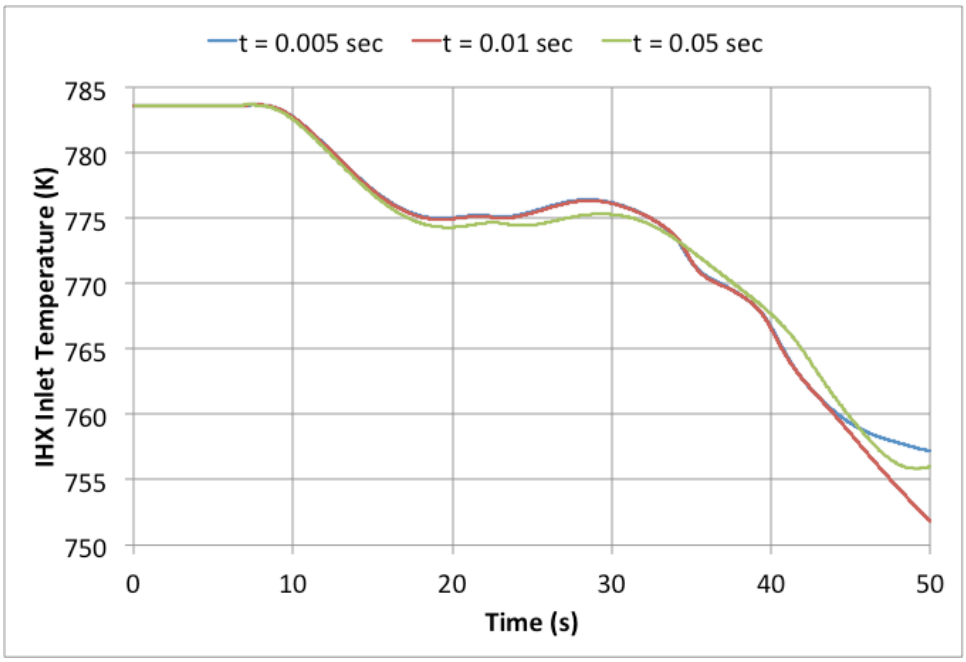

Figure 35: Predicted Temperature at the IHX Outlet in the Time Step Size Study

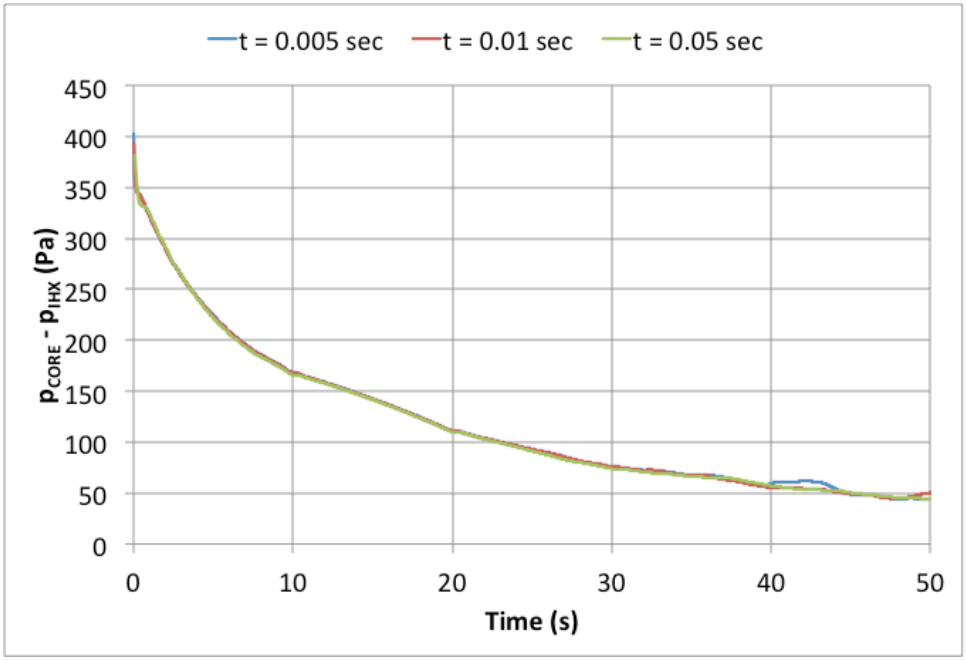

Figure 36: Pressure Difference between Core Outlet and IHX Inlet in the Time Step Size Study

5.3.2 Coupled Code simulation

From the investigation of time-step effects in stand-alone CFD simulation, it is confirmed that smaller time step should be selected tor accurate CFD simulation results. However, larger

time steps are preferred for running longer time of transient in a moderate real time. Therefore, the effects of time-step are investigated again in the coupled code simulations. The first 200 seconds of the PLOF transient were performed with two time step sizes, 0.01 s and 0.05 s. Note that it takes about 10 days to complete the simulation using 0.01 as the time-step size.

The main results of the coupled code simulations were compared in Figure 37-Figure 40 between the two simulations with different time-step sizes. The predicted core flow (Figure 37), core outlet temperature (Figure 38), core inlet plenum and cold pool temepratures (Figure 39), and maximum cald temperatures (Figure 40) are almost the same between the two simulations. However, the hot pool outlet temperatuers (Figure 38) were quite different after 50s into the transient. Additionally, oscillating hot pool outlet temepratures were predicted in both simulations, indicating the complex behaviors of the velocity fields in the hot pool during the transient. If one only focuses on the core behavior durign the transient, i.e. the peak clad/fuel temeprature, using a relative larger time-step is acceptable.

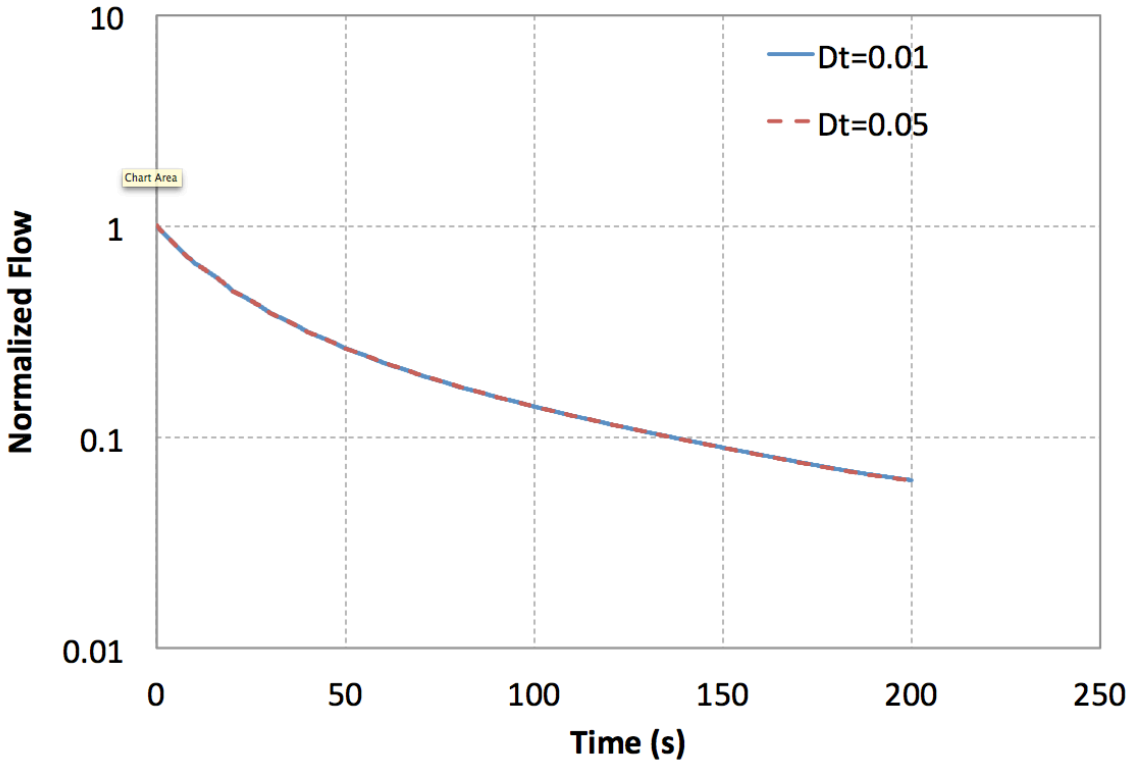

Figure 37: Normalized core flow in the coupled simulation, effects of time step size

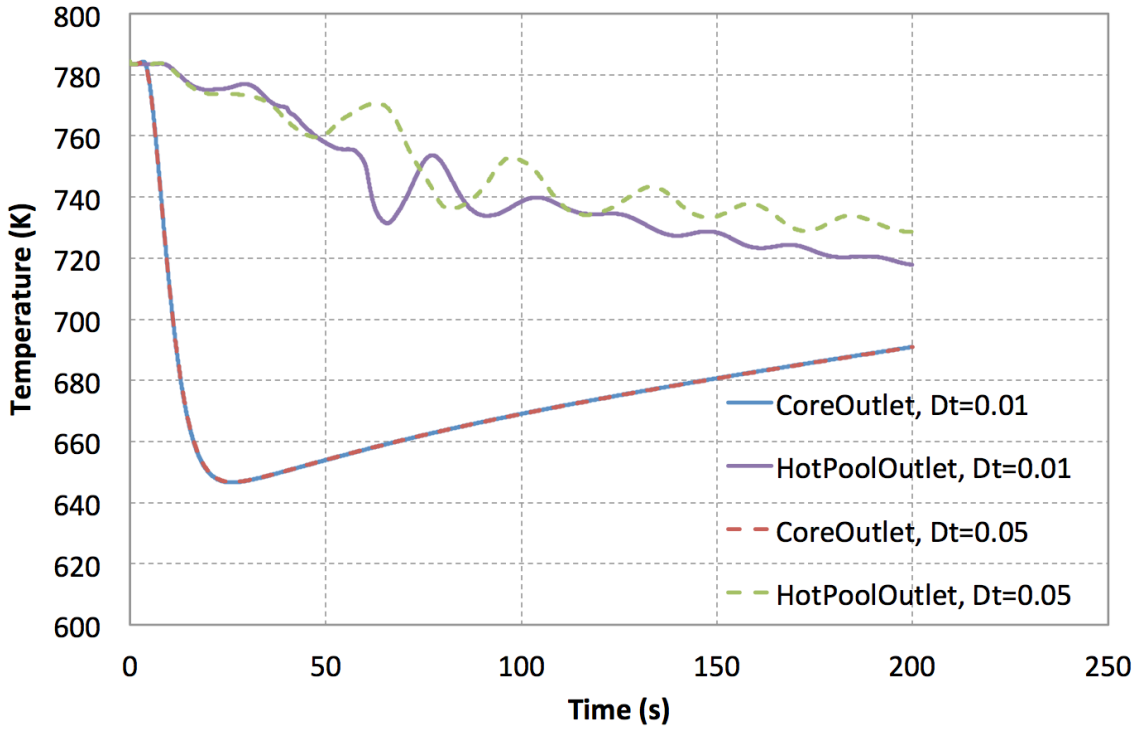

Figure 38: Hot pool inlet and outlet temperatures in the coupled simulation, effects of time step size

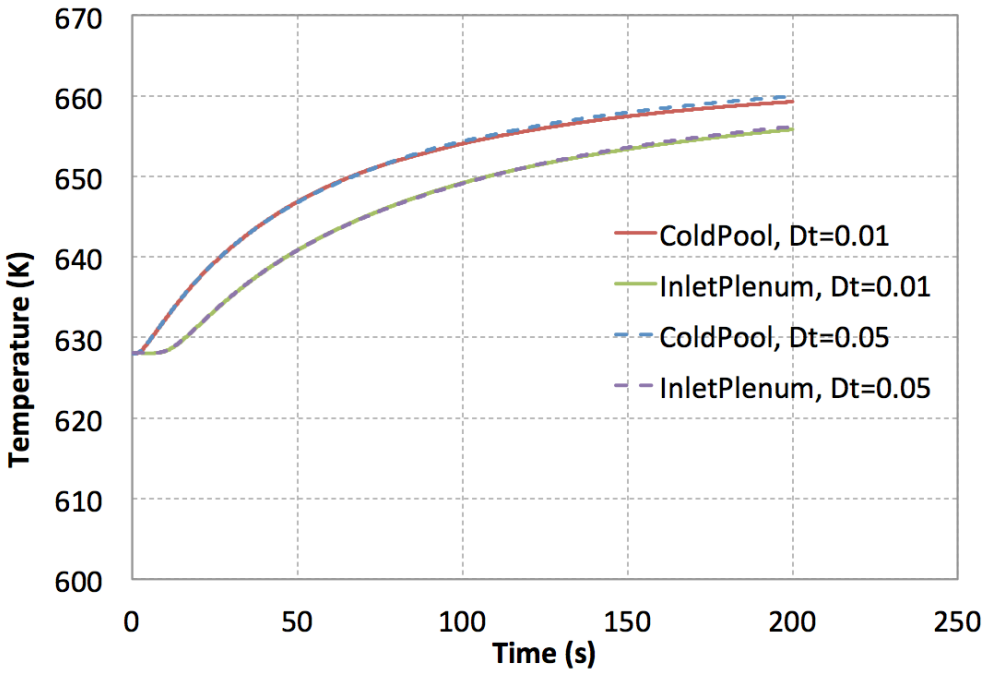

Figure 39: Cold pool and inlet plenum temperatures in the coupled simulation, effects of time step size

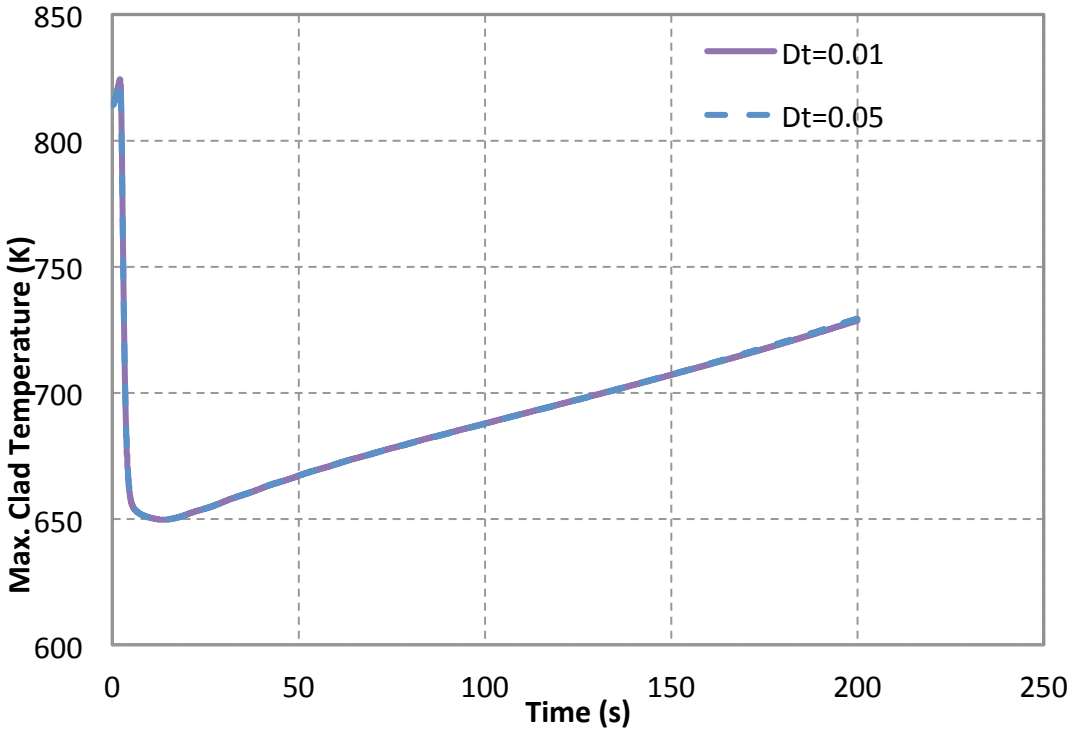

Figure 40: Maximum clad temperatures in the coupled simulation, effects of time step size

5.4 *Coupled Code Simulation of ABTR PLOF*

Based on the findings of the time-step effects discussed in Section 5.3, a variable time-step size scheme, shown in Figure 41, is used in the coupled code simulation of ABTR PLOF transient, for both accuracy and expediency of the transient simulation. Smaller time steps were used during the early stage when the flow velocity in the upper plenum is still high and experiencing fast changes; and larger time steps were used later the transient when the flow velocity is low and changes are small.

Results from coupled code simulation of the earlier PLOF transient during the pump coast down and transition to natural circulation are shown in Figure 42-Figure 47. The normalized core flow rate during the transient is compared with the stand-alone system code simulation in Figure 42. The transient flow behavior is similar in the two simulations, and the transitions to natural circulation flow are both very smooth. The core flow in the coupled code simulation is smaller after 200 seconds into the transient, but the natural circulation flow rates are similar in the two simulations.

The temperatures at the core inlet plenum, outlet plenum, and the cold pool are shown in Figure 43. The evolutions of the temperatures in these liquid volumes are found very similar, except the hot pool temperature. In the coupled code simulations, the three-dimensional flow and non-uniform temperature distribution in the hot pool are captured, and the hot pool outlet temperature could be very different from the inlet or the average temperature. In the stand-alone SFR Module simulation, a perfect mixing model is used for the hot pool, thus the hot pool outlet temperature is always the average temperature in the pool. After 200 seconds into the transient, the temperature in the lower part of hot pool of the coupled code simulation is significantly less than that of the system code simulation. This leads to increased gravity loss

in the hot pool, reduced overall driving head in the primary loop, thus smaller natural circulation flow rate in Figure 42. The maximum temperatures in the core during the transient are shown in Figure 44. The evolutions of the maximum temperatures are again very similar between the two simulations, except the higher peak temperatures in the coupled code simulations because of the lower predictions in core flow rate. Figure 45 shows the DRACS heat removal and the IHX heat removal rates. The similar behavior is found as that in the stand-alone system code simulation. Shortly after the transient is initiated, the DRACS operates at its capacity of removing 0.5% nominal power. As the cold pool temperature rises, DRACS heat removal capacity will increase accordingly. The intermediate heat transport system behaves alternately as a heat sink or source during the transient, depending on its temperature and the primary system temperature at the intermediate heat exchanger.

The evolutions of temperature distributions in the upper plenum during the transient are shown in Figure 46 and Figure 47 for the coupled code simulation. Immediately after the transient, the flow velocity is still very high and the clear jet path can be maintained at $t = 10\,s$. When the inlet flow continues dropping, the flow field in the upper plenum becomes very complex at $t = 28\,s$. The jet from the inlet can maintain for a short distance, and cold inlet sodium may enter into the lower annual region (spent fuel storage region) due to the buoyancy effect. The thermal stratification in the hot pool is clearly established when the inlet flow continues decreasing at $t = 60, 90, 200, 300\,s$. As the core outlet temperature continues rising, it becomes higher than the upper plenum temperature. The jet behavior appears again after at $t = 500\,s$. The complex flow field in the upper plenum causes the outlet temperature fluctuation during the transient, as seen in Figure 43. The temperature in the upper part of the upper plenum remains almost unchanged during the whole transient.

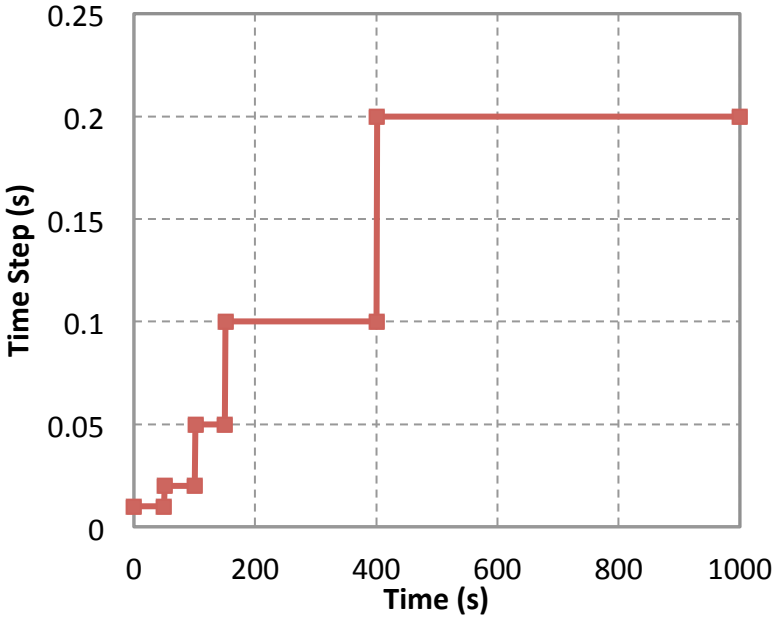

Figure 41: Time-step size scheme in the coupled simulation

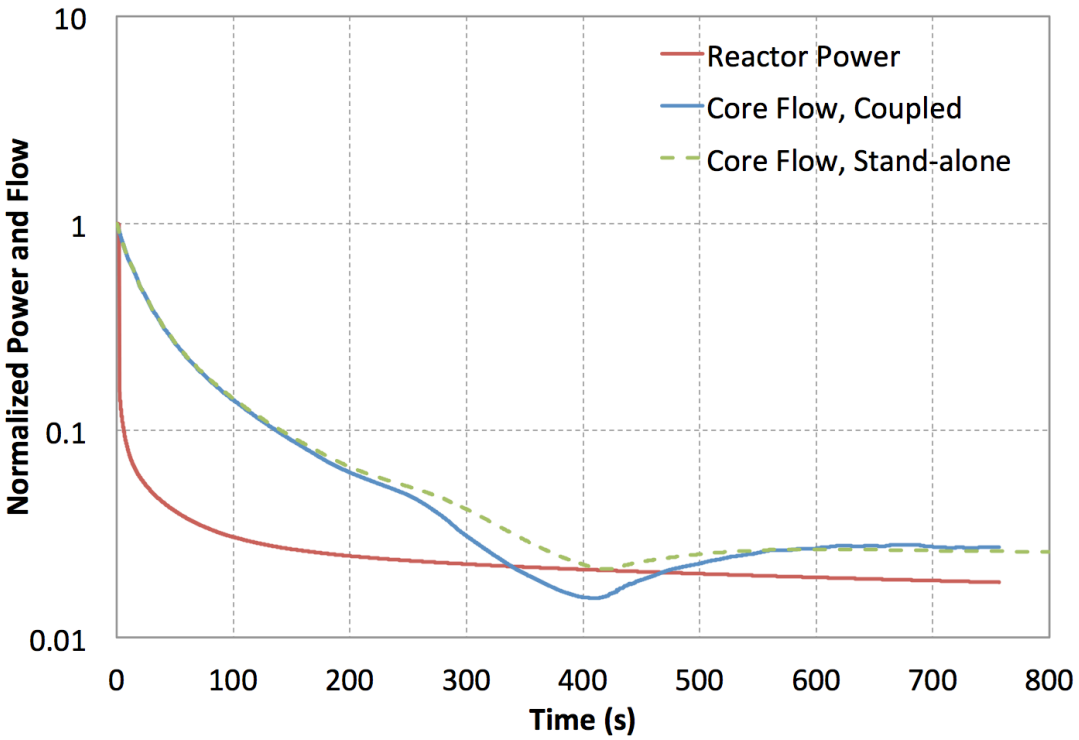

Figure 42: Normalized power and core flow in the coupled simulation

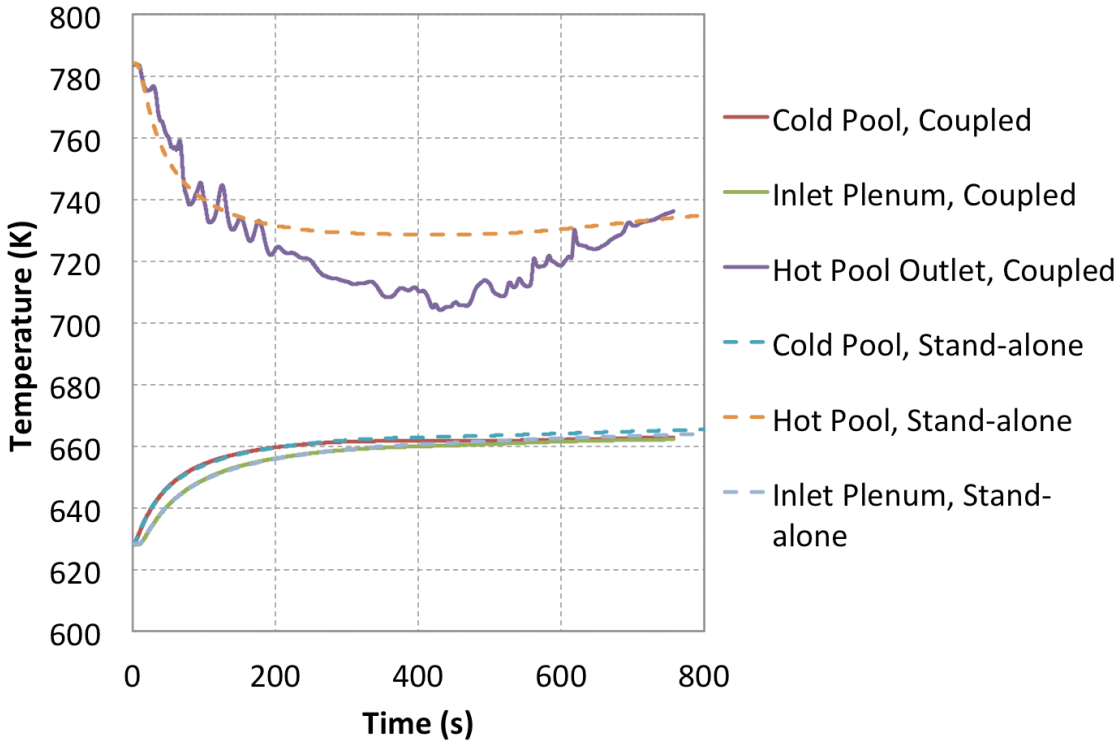

Figure 43: Pool temperatures in the coupled simulation

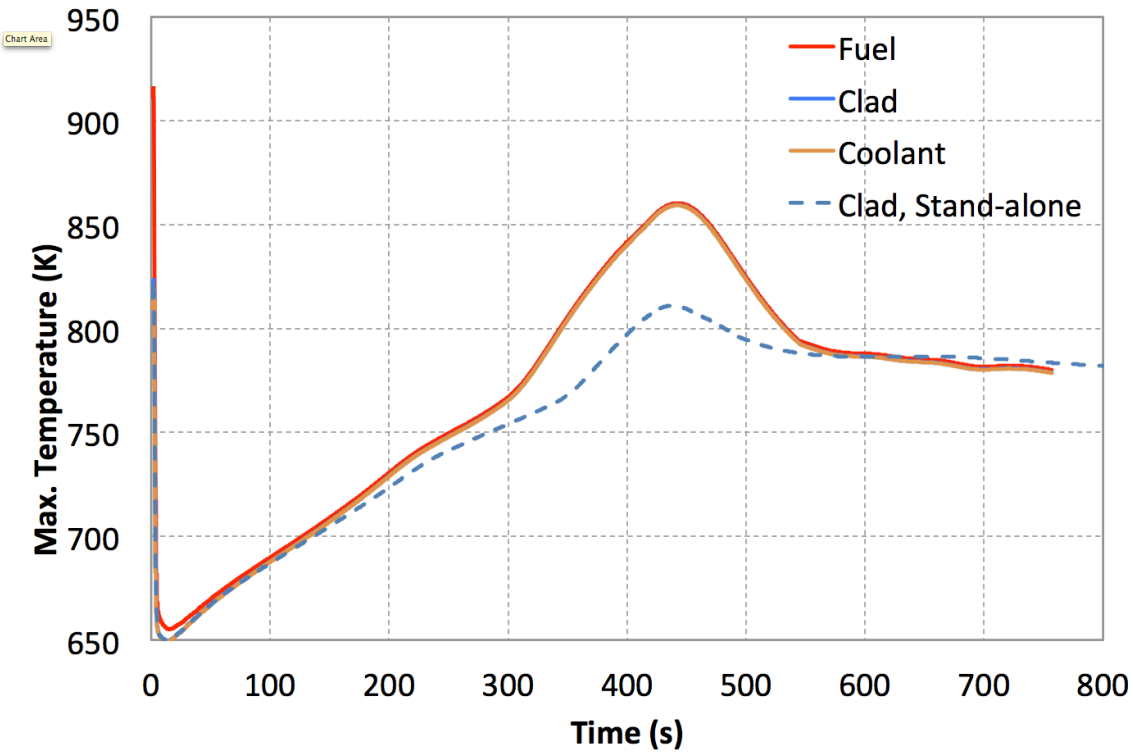

Figure 44: Core maximum temperatures in the coupled simulation

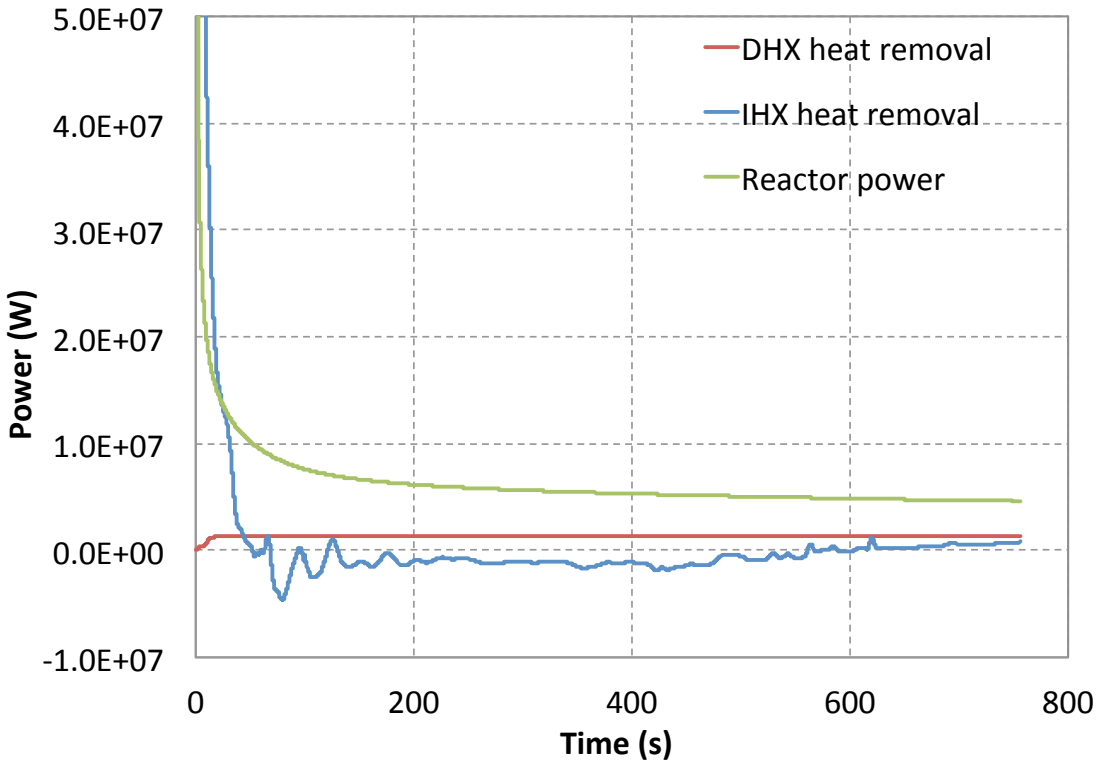

Figure 45: Heat removal rate in the coupled simulation

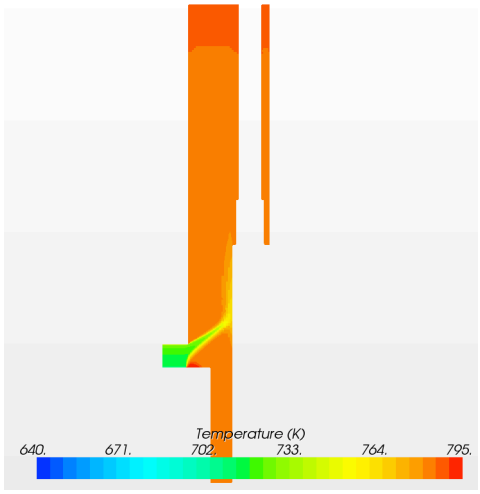

t = 10 s

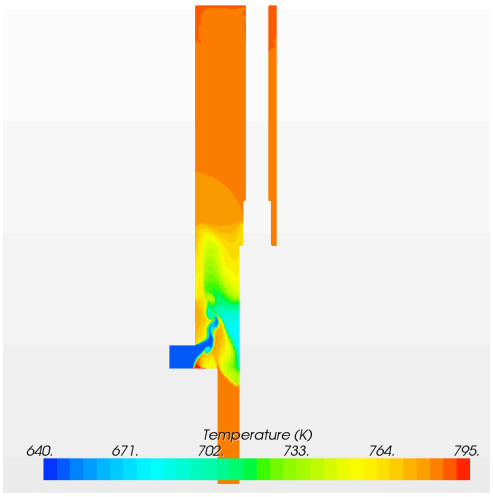

t = 28 s

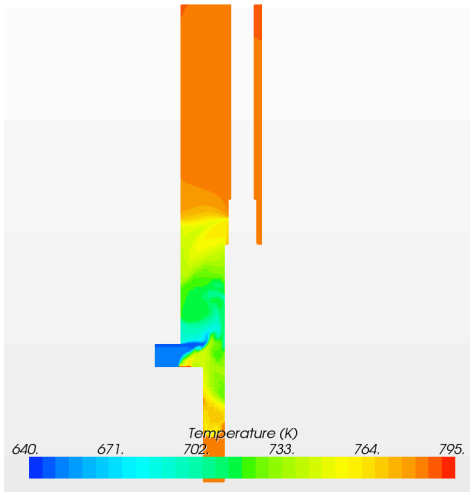

t = 40 s

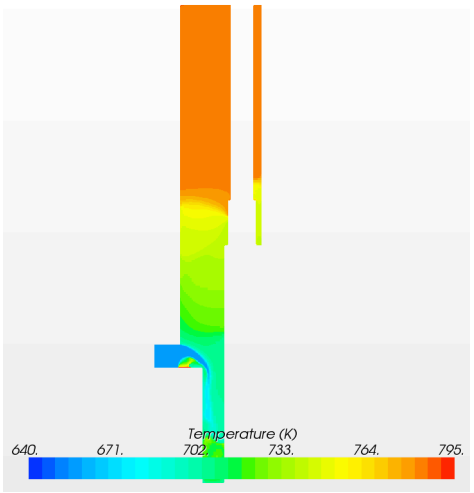

t = 60 s

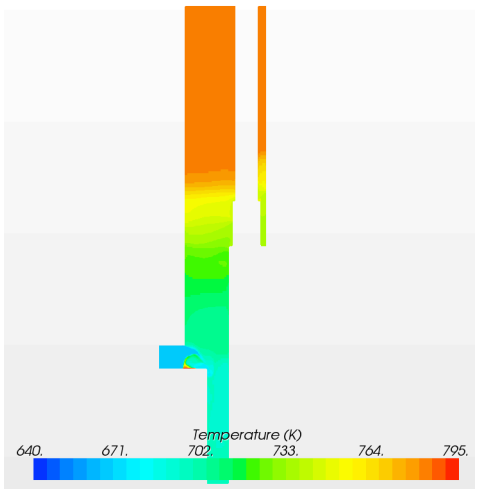

t = 90 s

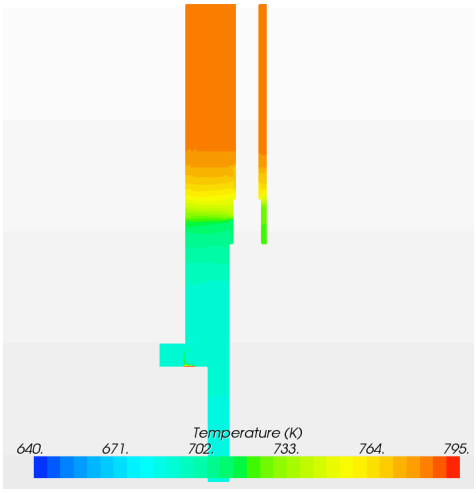

t = 200 s

Figure 46: CFD prediction of the temperature evolution during the early transient

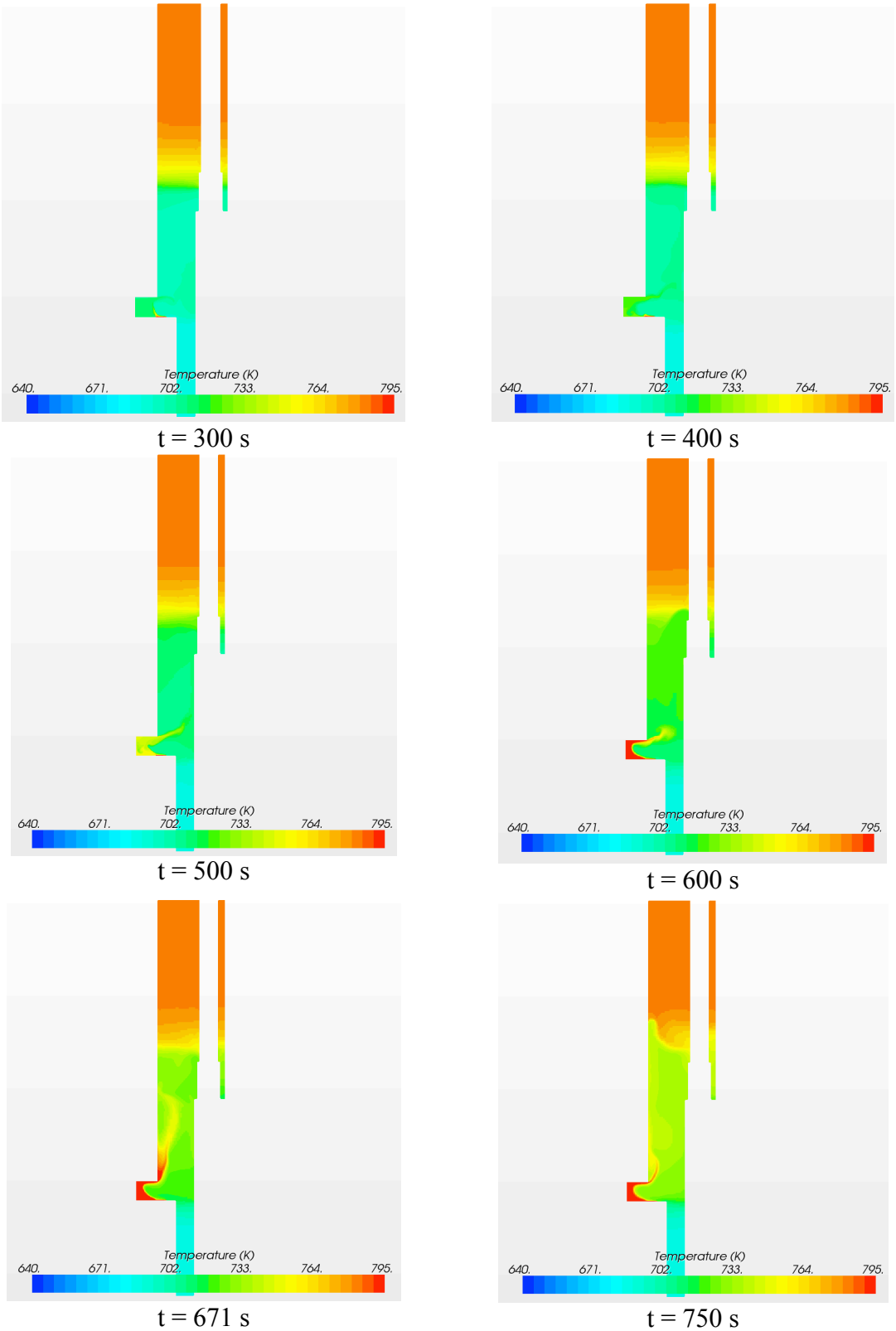

Figure 47: CFD prediction of the temperature evolution during the transient, $T \geq 300\ s$

5.5 Effects of UIS Modeling

The upper internal structure is approximated as a rounded cylinder with no flow inside in the above ABTR PLOF simulation. However, significant flow could enter into the UIS during normal and transient conditions. To investigate its effects to PLOF transient behavior, it is modeled as a porous medium in the CFD model. This avoids the detailed modeling of the complex geometry features such as the control rod guide tubes, instrumentations, and other miscellaneous structures. The interface between the UIS cylinder surface and the hot pool is modeled as a porous baffle. The resistance coefficients in the porous medium and at the porous baffle are taken from the study of a different SFR design. The velocity distributions in the upper plenum during normal operating conditions are shown in Figure 48. Very different velocity field is obtained if the UIS is included in the model. This would affect the transient evolution during the PLOF transient.

Results from coupled code simulation of the ABTR PLOF transient with the UIS modeled are shown in Figure 49 - Figure 53. The normalized core flow rate during the transient is compared with the simulation without UIS modeling in Figure 49. The transient flow behavior is similar in the two simulations, but the core flow rate is higher in the simulation with UIS modeled. The pressure differences between the core outlet and the IHX inlet are shown in Figure 50. It is seen that the pressure drop across the hot pool is smaller during the transient if the UIS is modeled, which leads to enhanced driving head in the primary loop and higher natural circulation flow rate.

The temperatures at the core inlet plenum, cold pool, hot pool inlet and outlet are shown in Figure 51 and Figure 52. The evolutions of the temperatures in the cold pool and core inlet plenum are found very similar. In the simulation with UIS modeled, the temperature predictions are higher in the cold pool and core inlet plenum, as more hot sodium flow into the cold pool through the IHX outlet. Because the cold pool temperature is higher, the DRACS heat removal rate is slight higher in the case with UIS modeled, as seen in Figure 53. The hot pool outlet temperature fluctuates in both simulations. However, if the UIS is modeled, the fluctuation is less severe, indicating less turbulence during the transient. In the case without UIS, the core outlet temperatures are significantly higher than the case with UIS modeled after 450 seconds into the transient, as seen in Figure 52, due to the lower predictions of the core flow.

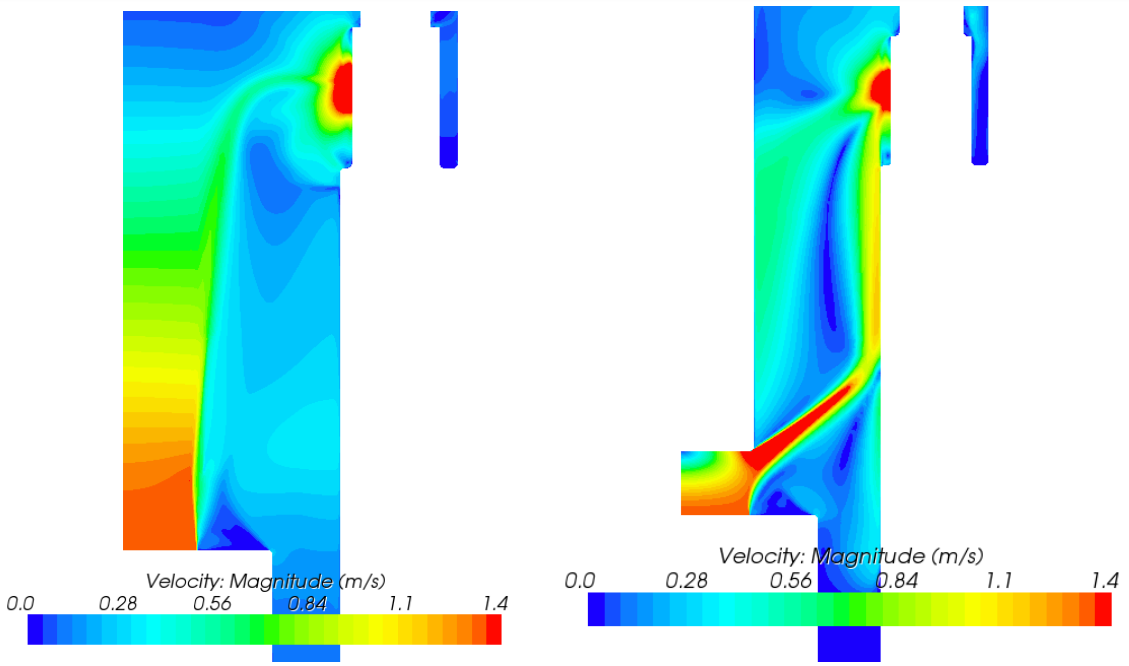

Figure 48: CFD prediction for the velocity fields prior to the initiation of PLOF, left: with UIS model; right: no UIS model

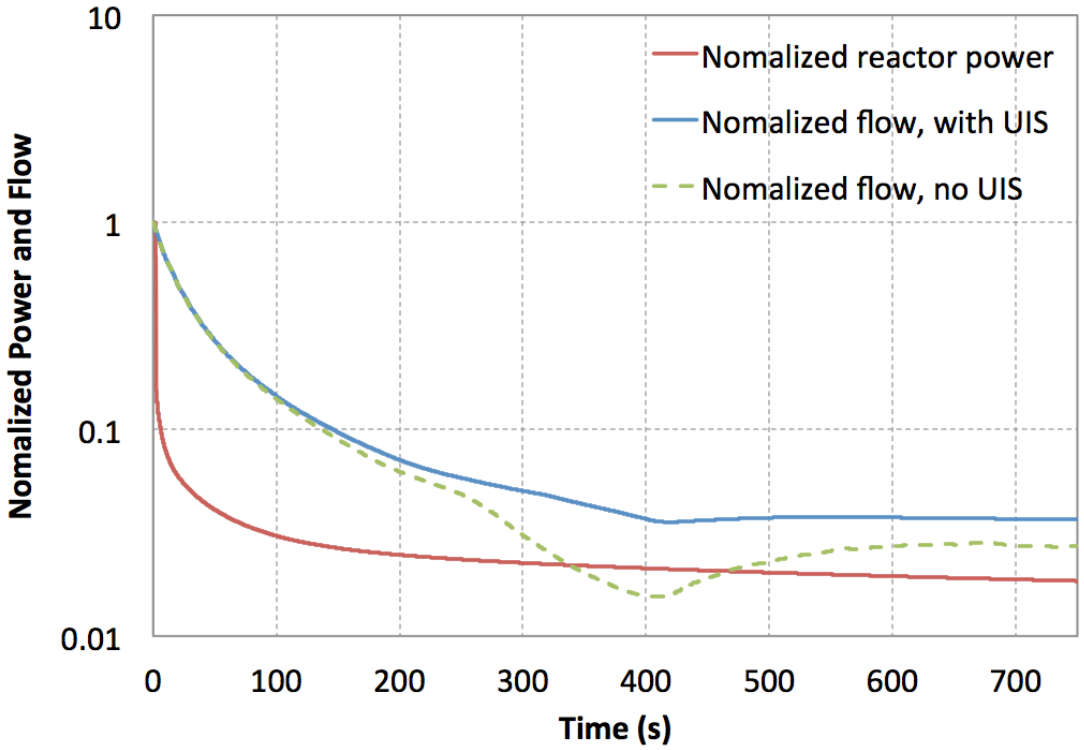

Figure 49: Normalized power and core flow in the coupled simulation, effects of UIS

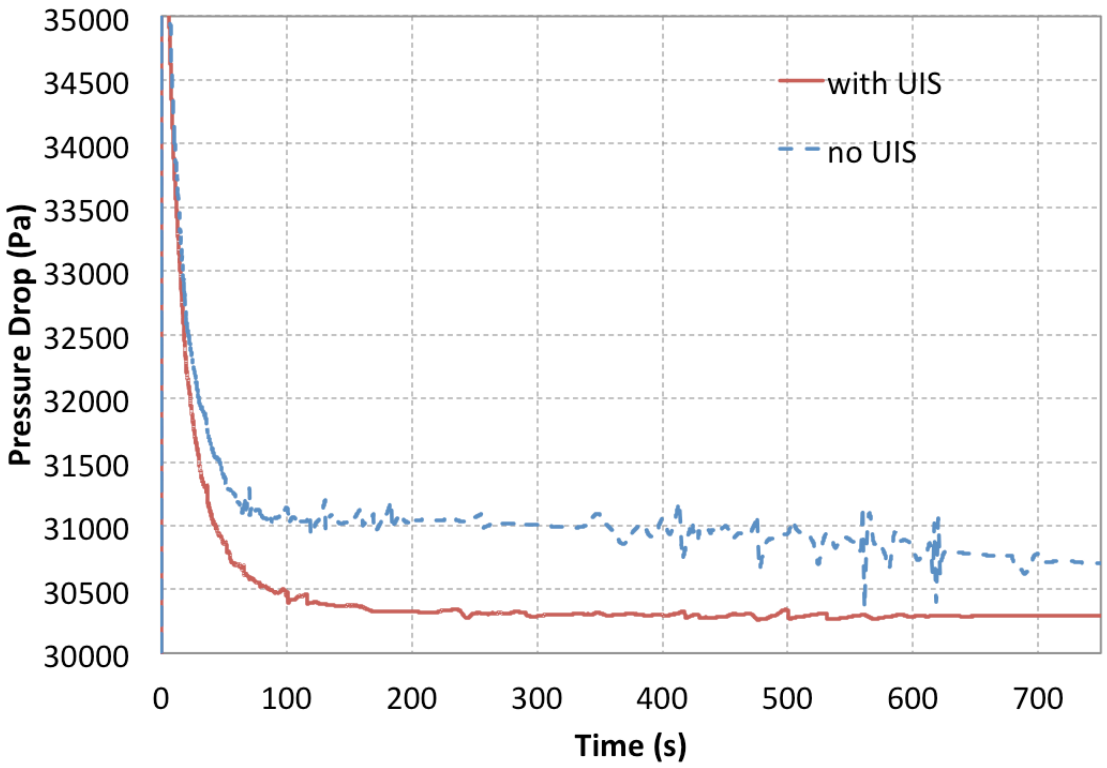

Figure 50: Pressure drop between the core outlet and hot pool outlet in the coupled simulation, effects of UIS

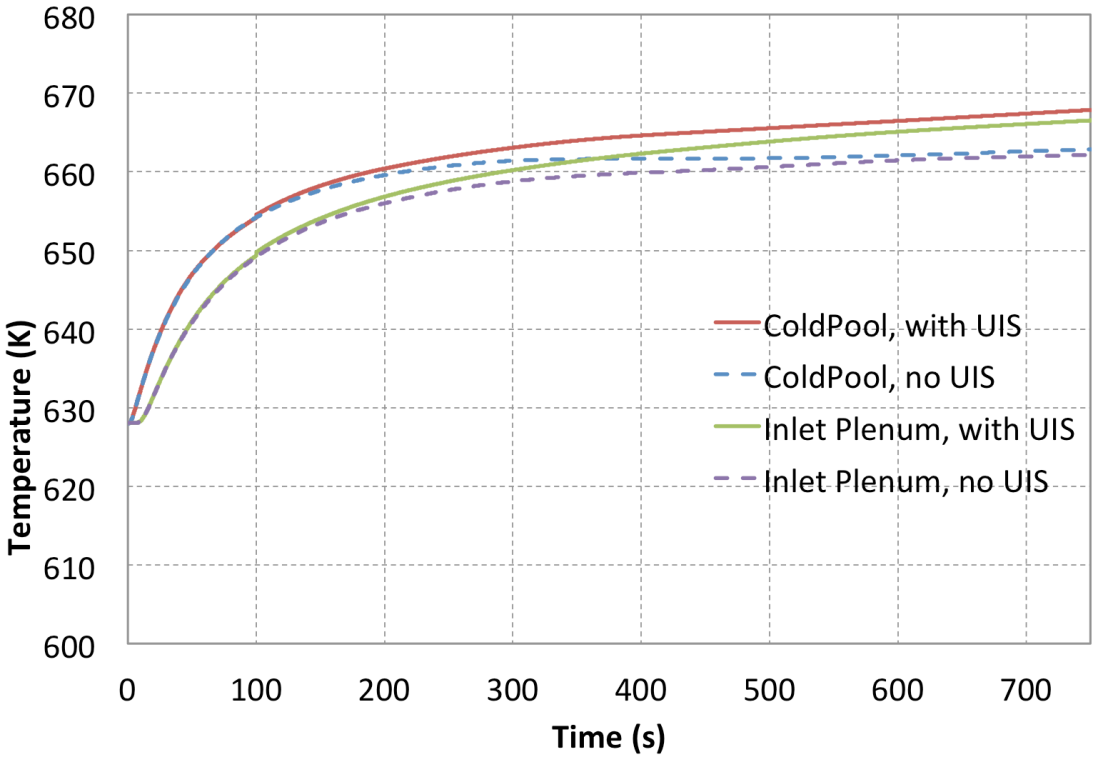

Figure 51: Liquid volume temperatures in the coupled simulation, effects of UIS

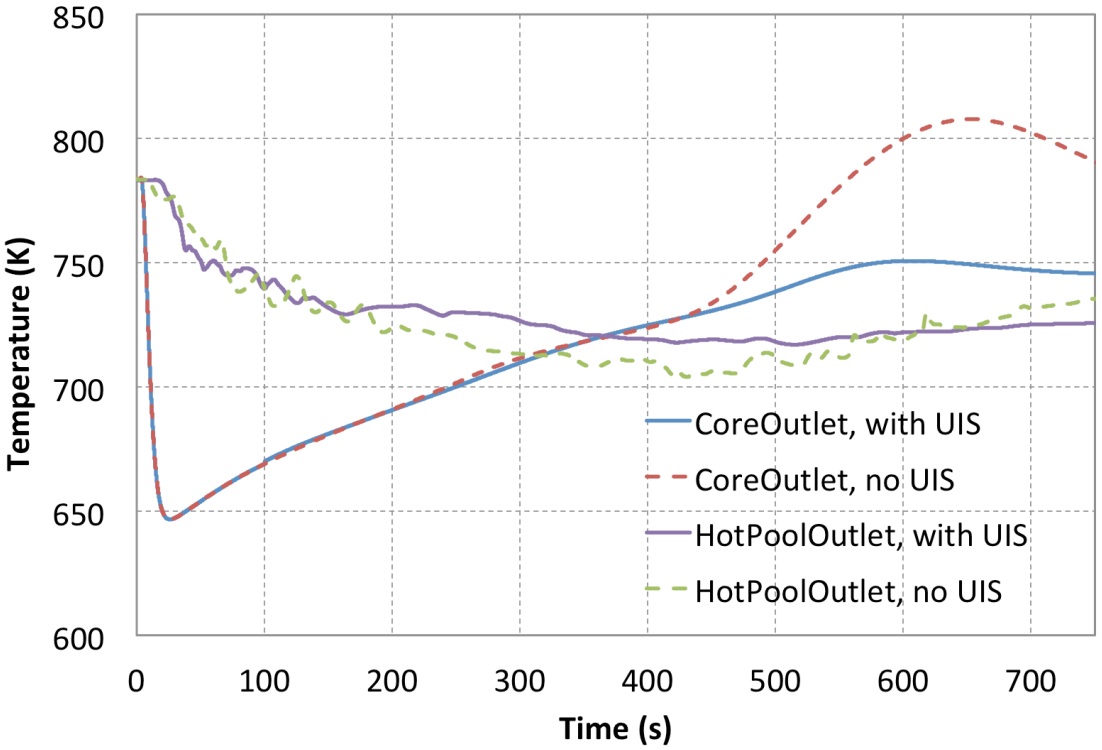

Figure 52: Temperatures at hot pool boundaries in the coupled simulation, effects of UIS

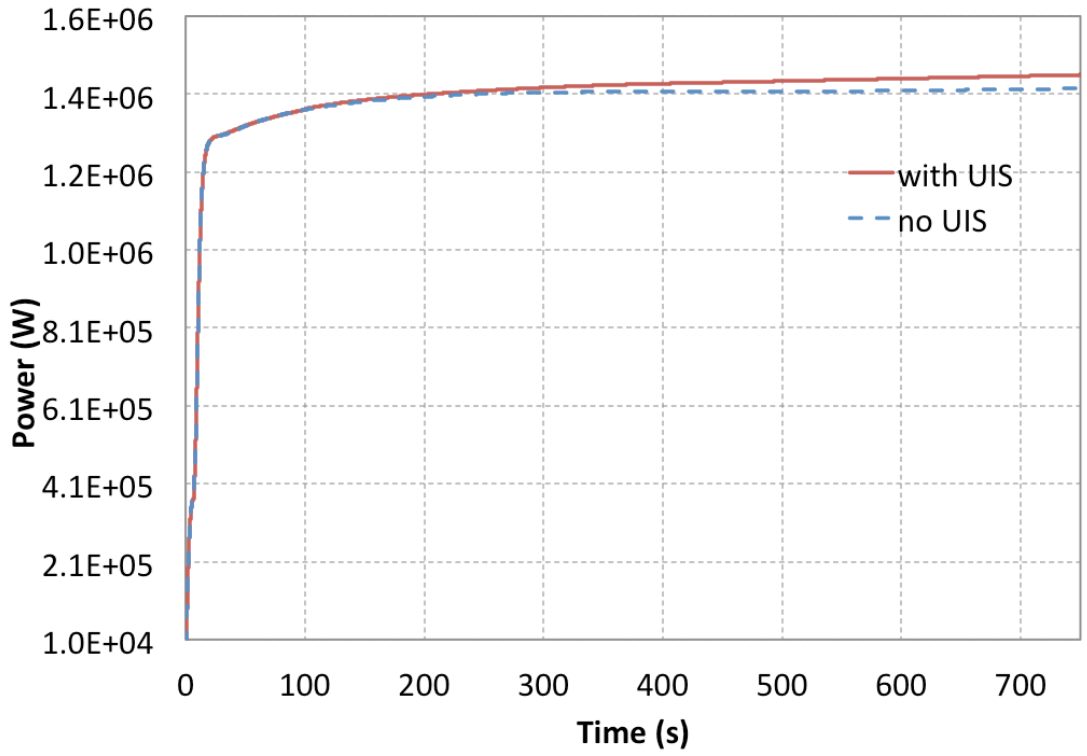

Figure 53: Heat removal rate from DHX in the coupled simulation, effects of UIS

6 Summary

The MOOSE and RELAP-7 based SFR system analysis module is currently under rapid development. Although it is a relative new effort (less than two years), significant accomplishments have been achieved. A 1-D FEM flow model using a primitive variable based formulation with numerical stabilization schemes has been developed for use in the incompressible sodium flows. A set of SFR-specific physics models and component has also been developed in addition to providing code verification and contributing general physics models and components applicable to all reactor types for RELAP-7 development. The simulation of the early stage of the ABTR PLOF transient has successfully demonstrated the SFR primary system simulation capabilities of the SFR Module. It is confirmed that major physics phenomena in the primary coolant loop during the transient can be captured by the SFR Module simulation.

The SFR module also emphasizes providing multi-scale multi-physics modeling capabilities by integrating with other higher-fidelity advanced simulation tools. The multi-scale coupling capability has been demonstrated in the coupled SFR Module and STAR-CCM+ code simulation of the ABTR PLOF transient. The importance of the multi-resolution capability was demonstrated by the multi-dimensional flow and the formation of thermal stratification layers in the outlet plenum and cold pool of the ABTR during the postulated transient. Although the general trends of transient evolutions are similar, very different flow and temperature magnitudes are predicted among the stand-alone SFR Module, stand-alone SAS4A/SASSYS-1, and the coupled SFR Module and STAR-CCM+ simulations because of the differences in modeling the mixing and thermal stratification in the large sodium pools. This investigation is important to the integration between the MOOSE-based system code and the high-fidelity and medium-fidelity advanced simulation capabilities developed under the NEAMS RPL. In the transient simulation of ABTR PLOF, the effects of “component-to-component” heat transfer, cold pool stratification, the modeling of upper internal structure (UIS), and the time-step size, have also been investigated. It is found that the PLOF transient response of the pool-type ABTR is sensitive to these modeling choices. Therefore, detailed CFD models of the cold pool, the hot pool, the redan wall, and the UIS are necessary for accurate predictions of the transient evolution in the coupled system and CFD code simulation of the ABTR PLOF.

Although significant progress has been made, the MOOSE-based system code development remains a challenging task, partly due to the first-of-a-kind development of a FEM-based multi-physics nuclear system analysis capability. It is important to continue the collaborative effort on the development of RELAP-7 and the SFR Module, which will help advance the system modeling and simulation capabilities for both LWRs and advanced reactor concepts.

Following on the success of the FY2013 collaboration, Argonne developers will focus on continued development of physics modeling and component designs for SFR analysis, and on demonstrating the preliminary code capability through additional simulation of SFR design base accidents, such as the unprotected loss-of-flow (ULOF) accident. Further investigation will also address the possible integration between the primitive variable based formulation and the conservative variable based formulation in RELAP-7 so that both flow models can be used in a single simulation. Additionally, the integration with other high-fidelity advanced simulation tools developed under the NEAMS Program, such as Nek-5000, will be

investigated. Finally, advanced preconditioning techniques or alternative numerical integration schemes other than JFNK will be explored to improve the code execution speed.

REFERENCES

[1] D. Gaston, C. Newman, G. Hansen, and D. Lebrun-Grandi´e, "MOOSE: A parallel computational framework for coupled systems of nonlinear equations," Nuclear Engineering and Design, vol. 239, pp. 1768–1778, (2009).

[2] B. S. Kirk, J. W. Peterson, R. H. Stogner, and G. F. Carey, "libMesh: A C++ Library for Parallel Adaptive Mesh Refinement/Coarsening Simulations," Engineering with Computers, 22(3-4): 237-254, (2006).

[3] S. Balay, J. Brown, K. Buschelman, V. Eijkhout, W. D. Gropp, D. Kaushik, M. G. Knepley, L. C. McInnes, B. F. Smith, and H. Zhang, "PETSc Users Manual, ANL-95/11 – Revision 3.3," Argonne National Laboratory, (2012).

[4] D. Anders, R. Berry, D. Gaston, et al., "Demonstration of a Steady State Single Phase PWR Simulation with RELAP-7", INL/EXT-12-25924, Idaho National Laboratory, May (2012).

[5] CD-adapco, "STAR-CCM+ 7.06 Manual," N.Y., (2012).

[6] Y. I. Chang, P. J. Finck, C. Grandy, et al., "Advanced Burner Test Reactor Preconceptual Design Report," ANL-ABR-1 (ANL-AFCI-173), Argonne National Laboratory, September (2006).

[7] T. H. Fanning, ed., The SAS4A/SASSYS-1 Safety Analysis Code System, Argonne National Laboratory, ANL/NE-12/4, January 31, (2012).

[8] RELAP5-3D Code Manual Volume 1: Code Structure, System Models and Solution Methods, INEEL-EXT-98-00834, Rev. 4, June (2012), http://www.inl.gov/relap5.

[9] R. C. Martineau, The PCICE-FEM Scheme for Highly Compressible Axisymmetric Flows, Computers & Fluids, Vol. 36, p. 1259, (2007).

[10] R. A. Berry and R. C. Martineau, Examination of the PCICE Method in the Nearly Incompressible, as well as Strictly Incompressible, Limits, ICONE15-10278 Proceedings of ICONE15, The 15th International Conference on Nuclear Engineering, Nagoya, Japan, April 22-26, (2007).

[11] R.C. Martineau and R. A. Berry, The Pressure-Corrected ICE Finite Element Method (PCICE-FEM) for Compressible Flows on Unstructured Meshes, Journal of Computational Physics, Vol. 198, p. 659, (2004).

[12] R.A. Berry and S.Y. Kadioglu, "All-Speed Methods and Long-Duration Time Integration for Incorporation into the 7-Equation Two-Phase", INL/EXT-12-25997, Idaho National Laboratory, May (2012).

[13] T.E. Tezduyar, "Stabilized Finite Element Formulations for Incompressible Flow Computations," Advances in Applied Mechanics, Vol. 28, 1-44, (1992)

[14] N.E. Todreas and M.S. Kazimi, "Nuclear Systems I – Thermal Hydraulic Fundamentals," Hemisphere Publishing Corporation, (1990)

[15] T.H. Fanning and J.W. Thomas, "Integration of CFD into Systems Analysis Codes for Modeling Thermal Stratification during SFR Transients," Proceedings of NURETH-14, Toronto, Ontario, Canada, September 25-30, (2011).

[16] Rui Hu, Justin W. Thomas, and Thomas H. Fanning, "Strategy for Multi-Scale Single-Phase Flow Coupling," ANL/NE-13/4, Argonne National Laboratory, March (2013).

Nuclear Engineering Division
Argonne National Laboratory
9700 South Cass Avenue
Argonne, IL 60439

www.anl.gov

Argonne National Laboratory is a U.S. Department of Energy laboratory managed by UChicago Argonne, LLC